

## Mechanisms of water supply and vegetation demand govern the seasonality and magnitude of evapotranspiration in Amazonia and Cerrado



Bradley O. Christoffersen<sup>a,b,\*</sup>, Natalia Restrepo-Coupe<sup>a,c</sup>, M Altaf Arain<sup>d</sup>, Ian T. Baker<sup>e</sup>, Bruno P. Cestaro<sup>f</sup>, Phillippe Ciais<sup>g</sup>, Joshua B. Fisher<sup>h</sup>, David Galbraith<sup>i,j</sup>, Xiaodan Guan<sup>k</sup>, Lindsey Gulden<sup>k,l</sup>, Bart van den Hurk<sup>m</sup>, Kazuhito Ichii<sup>n</sup>, Hewlley Imbuzeiro<sup>o</sup>, Atul Jain<sup>p</sup>, Naomi Levine<sup>q</sup>, Gonzalo Miguez-Macho<sup>r</sup>, Ben Poulter<sup>s</sup>, Debora R. Roberti<sup>t</sup>, Koichi Sakaguchi<sup>b</sup>, Alok Sahoo<sup>u</sup>, Kevin Schaefer<sup>v</sup>, Mingjie Shi<sup>k</sup>, Hans Verbeeck<sup>w</sup>, Zong-Liang Yang<sup>k</sup>, Alessandro C. Araújo<sup>x</sup>, Bart Kruijt<sup>y</sup>, Antonio O. Manzi<sup>z</sup>, Humberto R. da Rocha<sup>f</sup>, Celso von Randow<sup>aa</sup>, Michel N. Muza<sup>bb</sup>, Jordan Borak<sup>cc</sup>, Marcos H. Costa<sup>o</sup>, Luis Gustavo Gonçalves de Gonçalves<sup>bb,cc</sup>, Xubin Zeng<sup>b</sup>, Scott R. Saleska<sup>a</sup>

<sup>a</sup> Department of Ecology and Evolutionary Biology, University of Arizona, Tucson, AZ, USA

<sup>b</sup> Department of Atmospheric Sciences, University of Arizona, Tucson, AZ, USA

<sup>c</sup> Plant Functional Biology and Climate Change Cluster, University of Technology, Sydney, Australia

<sup>d</sup> School of Geography and Earth Sciences, McMaster University, Hamilton, ON, Canada

<sup>e</sup> Atmospheric Science Department, Colorado State University, Fort Collins, CO, USA

<sup>f</sup> Departamento de Ciências Atmosféricas, IAG, Universidade de São Paulo, São Paulo, Brazil

<sup>g</sup> LSCE CEA-CNRS-UVSQ, Orme des Merisiers, F-91191 Gif-sur-Yvette, France

<sup>h</sup> Jet Propulsion Laboratory, California Institute of Technology, Pasadena, CA, USA

<sup>i</sup> Environmental Change Institute, School of Geography and the Environment, University of Oxford, Oxford OX1 3QY, UK

<sup>j</sup> School of Geography, University of Leeds, Leeds, UK

<sup>k</sup> Center for Integrated Earth System Science, Department of Geological Sciences, The University of Texas at Austin, Austin, TX, USA

<sup>l</sup> ExxonMobil Upstream Research Company, Houston, TX, USA

<sup>m</sup> Royal Netherlands Meteorological Institute (KNMI), De Bilt, Netherlands

<sup>n</sup> Faculty of Symbiotic Systems Science, Fukushima University, Japan

<sup>o</sup> Dep Agricultural Engineering, Federal University of Viçosa, Viçosa, MG, Brazil

<sup>p</sup> Department of Atmospheric Sciences, University of Illinois at Urbana-Champaign, Urbana, IL, USA

<sup>q</sup> Department of Organismic and Evolutionary Biology, Harvard University, Cambridge, MA, USA

<sup>r</sup> Physics Faculty, Universidade de Santiago de Compostela, Santiago de Compostela, Galicia, Spain

<sup>s</sup> Swiss Federal Research Institute WSL, Dynamic Macroecology, Birmensdorf, Switzerland

<sup>t</sup> Dept of Physics, Federal University of Santa Maria, Santa Maria, RS, Brazil

<sup>u</sup> Center for Research on Environment and Water, IGES, Calverton, MD, USA

<sup>v</sup> National Snow and Ice Data Center, Cooperative Institute for Research in Environmental Sciences, University of Colorado at Boulder, Boulder, CO 80309, USA

<sup>w</sup> Laboratory of Plant Ecology, Ghent University, Ghent, Belgium

<sup>x</sup> Embrapa Amazônia Oriental, Belém, PA, Brazil

<sup>y</sup> Wageningen University & Research Center, Wageningen, Netherlands

<sup>z</sup> Instituto Nacional de Pesquisas da Amazônia (INPA), Manaus, AM, Brazil

<sup>aa</sup> Centro de Ciência do Sistema Terrestre (CCST), Instituto Nacional de Pesquisas Espaciais (INPE), Cachoeira Paulista, SP, Brazil

<sup>bb</sup> Earth System Science Interdisciplinary Center, University of Maryland, College Park, Hydrological Sciences Laboratory, NASA Goddard Space Flight Center, USA

<sup>cc</sup> Centro de Previsão de Tempo e Estudos Climáticos (CPTEC), Instituto Nacional de Pesquisas Espaciais (INPE), Cachoeira Paulista, SP, Brazil

### ARTICLE INFO

#### Article history:

Received 14 August 2013

Received in revised form 4 February 2014

Accepted 17 February 2014

Available online 15 March 2014

### ABSTRACT

Evapotranspiration ( $E$ ) in the Amazon connects forest function and regional climate via its role in precipitation recycling. However, the mechanisms regulating water supply to vegetation and its demand for water remain poorly understood, especially during periods of seasonal water deficits. In this study, we

\* Corresponding author at: Present address: School of GeoSciences, Crew Building, King's Buildings, University of Edinburgh, Edinburgh EH9 3JN, UK. Tel.: +1 520 626 5838; fax: +1 520 621 9190.

E-mail addresses: [bchristo@email.arizona.edu](mailto:bchristo@email.arizona.edu), [bradleychristo@gmail.com](mailto:bradleychristo@gmail.com) (B.O. Christoffersen).

**Keywords:**

Tropical forest  
 Evapotranspiration  
 Deep roots  
 Groundwater  
 Canopy stomatal conductance  
 Intrinsic water use efficiency

address two main questions: First, how do mechanisms of water supply (indicated by rooting depth and groundwater) and vegetation water demand (indicated by stomatal conductance and intrinsic water use efficiency) control evapotranspiration ( $E$ ) along broad gradients of climate and vegetation from equatorial Amazonia to Cerrado, and second, how do these inferred mechanisms of supply and demand compare to those employed by a suite of ecosystem models? We used a network of eddy covariance towers in Brazil coupled with ancillary measurements to address these questions. With respect to the magnitude and seasonality of  $E$ , models have much improved in equatorial tropical forests by eliminating most dry season water limitation, diverge in performance in transitional forests where seasonal water deficits are greater, and mostly capture the observed seasonal depressions in  $E$  at Cerrado. However, many models depended universally on either deep roots or groundwater to mitigate dry season water deficits, the relative importance of which we found does not vary as a simple function of climate or vegetation. In addition, canopy stomatal conductance ( $g_s$ ) regulates dry season vegetation demand for water at all except the wettest sites even as the seasonal cycle of  $E$  follows that of net radiation. In contrast, some models simulated no seasonality in  $g_s$ , even while matching the observed seasonal cycle of  $E$ . We suggest that canopy dynamics mediated by leaf phenology may play a significant role in such seasonality, a process poorly represented in models. Model bias in  $g_s$  and  $E$ , in turn, was related to biases arising from the simulated light response (gross primary productivity,  $GPP$ ) or the intrinsic water use efficiency of photosynthesis ( $iWUE$ ). We identified deficiencies in models which would not otherwise be apparent based on a simple comparison of simulated and observed rates of  $E$ . While some deficiencies can be remedied by parameter tuning, in most models they highlight the need for continued process development of belowground hydrology and in particular, the biological processes of root dynamics and leaf phenology, which via their controls on  $E$ , mediate vegetation–climate feedbacks in the tropics.

© 2014 Elsevier B.V. All rights reserved.

## 1. Introduction

Evapotranspiration ( $E$ ) in the Amazon is the dominant connection between forest function and regional climate, primarily through its role in precipitation recycling (Victoria et al., 1991; Eltahir and Bras, 1994). Global circulation model (GCM) studies which simulate the effects of deforestation have shown a reduction of rainfall downwind (Walker et al., 1995), implying a coupling between the integrity of the Amazonian hydrometeorological system and forest function. Such a coupling presents an opportunity for a positive feedback under climate change: should future rainfall in the Amazon decrease and forests downregulate metabolism via stomatal closure, rainfall reductions basin-wide could be exacerbated and further threaten forest integrity (Betts et al., 2004). Loss of a significant area of Amazon forest due to climate change, deforestation, or a combination of both can have further impacts globally due to hydrometeorological teleconnections (Werth and Avissar, 2002) or carbon cycle feedbacks (Cox et al., 2000). However, much uncertainty remains surrounding modeling forest response to climate anomalies, due to both to model process differences/parameters or due to uncertainty in climate projections (Huntingford et al., 2008; Sitch et al., 2008; Galbraith et al., 2010; Poulter et al., 2012). This paper seeks to further investigate model process uncertainty by focusing on mechanisms controlling the seasonality and magnitude of  $E$  in the Amazon basin using a data–model intercomparison approach (de Gonçalves et al., 2013).

Recent syntheses using data from eddy covariance measures of carbon, water, and energy exchange across Amazonia indicate a simple dependency of  $E$  on net radiation ( $R_n$ ) for forest types ranging from seasonally wet to seasonally dry forests (Shuttleworth, 1988; Hasler and Avissar, 2007; Juarez et al., 2007; da Rocha et al., 2002, 2009; Fisher et al., 2009). However, this stands in stark contrast to many model predictions which instead have historically simulated an annual  $E$  cycle in phase with precipitation ( $P$ ) (Shuttleworth, 1991; Bonan, 1998; Dickinson et al., 2006), suggesting that  $E$  is limited by water availability. Such a discrepancy between models and data indicates that knowledge of the mechanisms which regulate  $E$  remain poorly understood.

Uncertainty in ecosystem land surface models (LSMs) with respect to  $E$  fluxes can be broadly grouped into those aspects

relating to the supply of water to vegetation belowground and those involved in vegetation response to changes in water supply. In recent years, attention has been almost singularly focused on fixing the supply side of the problem, implementing deep soil and/or deep roots (Ichii et al., 2007; Baker et al., 2008; Grant et al., 2009; Harper et al., 2010; Verbeeck et al., 2011), root hydraulic redistribution (Lee et al., 2005), unconfined aquifers (Oleson et al., 2008; Fan and Miguez-Macho, 2010; Miguez-Macho and Fan, 2012), or changes to the numerical solution of the Richards equation for soil water fluxes (Zeng and Decker, 2009) to improve seasonal patterns of soil moisture and/or the seasonality of ecosystem metabolism. Despite the attention given to these ecohydrological mechanisms, little is known as to the relative contribution of soil physical versus biological mechanisms mediating supply.

On the other hand, control of the demand of water by vegetation in response to changes in water supply may be an equally important mechanism regulating the seasonality and magnitude of  $E$ . These have received comparatively less attention as a focus for model improvements. Canopy stomatal conductance and intrinsic water use efficiency ( $iWUE$ ) are two key mechanisms controlling vegetation demand for water, respectively, in relation to atmospheric vapor pressure deficit ( $D$ ) and ecosystem photosynthesis ( $GPP$ ) arising from the ‘photosynthesis–transpiration’ compromise (Lloyd et al., 2002; Beer et al., 2009). The degree to which stomata regulate transpiration ( $E_t$ ) independent of environmental conditions in the Amazon has been the topic of debate (Avissar and Werth, 2004; Costa et al., 2004). The conclusions of syntheses of eddy covariance measures of the seasonality of  $E$  in the Amazon have largely emphasized the secondary role of vegetation demand across a range of forest types (Costa et al., 2004; Juarez et al., 2007; da Rocha et al., 2002, 2009; Fisher et al., 2009), but recent work suggests that forests indeed exhibit varying degrees of control on the seasonal exchange of water in their canopies (Costa et al., 2010). Much of what is known about the functioning of stomata remains phenomenological; at the leaf-level, attempts at forming a solid mechanistic basis of stomatal function have proven to be a challenge (Buckley, 2005; Peak and Mott, 2011).

The range of control points for  $E$  within the soil–plant–atmosphere continuum calls for a critical assessment of the ‘state-of-art’ mechanisms employed to predict  $E$  in ecosystem LSMs. We do so by addressing those involved in both the supply

(belowground) and demand (aboveground) side. To be clear, the environment and vegetation both control aspects of supply and demand, the former being regulated by soil water and the root networks which exploit it (ecohydrological mechanisms) and the latter regulated both by the atmosphere (e.g., net radiation and vapor pressure deficit) and stomata (the latter representing eco-physiological mechanisms). This paper seeks to disentangle the relative role of abiotic and biotic controls on both supply and demand, and use these findings to evaluate modeled  $E$ .

We begin with a data-model comparison of the magnitude and seasonality of  $E$  from equatorial Amazonia to Cerrado and its first-order correlation with available energy (i.e., do models get the right answer?). This motivates a second-order analysis of supply and demand from observational and modeling perspectives (i.e., what are the mechanisms, and do models get the right answer for the right reasons?). With respect to water supply, we discriminate between the relative roles of capillary flux from groundwater (a physical mechanism; “bringing the water to the trees”) and roots penetrating deep into the soil (a biological mechanism; “taking the trees to the water”) in regulating  $E$  during seasonal water deficits. Next, with respect to vegetation demand for water, we assess how seasonal patterns of canopy stomatal conductance impact the seasonality of  $E$ , and how canopy intrinsic water use efficiency ( $iWUE$ ); photosynthesis per unit evaporative potential of water through stomata) mediates the relationship between gross photosynthesis ( $GPP$ ) and  $E$ . We use the available data to answer these questions while evaluating the suite of models with respect to these mechanisms of supply and demand. Finally, we derive a simple model benchmark which incorporates both right answer/right reason aspects of data-model intercomparison.

## 2. Materials and methods

### 2.1. Site descriptions, grouping, and observational data

We selected five forest sites and one Cerrado site from a network of eddy covariance towers in Brazil called ‘BrasilFlux’ (Restrepo-Coupe et al., 2013), where measurements of climate and the turbulent exchange of water, carbon, and momentum at the ecosystem level had been made. General characteristics of the vegetation, climate, and soil at each site are given in Table 1. We grouped sites into three site groups based on similarities in the seasonality of precipitation ( $P$ ) as well as net radiation ( $R_n$ ) and latitude: equatorial evergreen forests (K34, K67, K83 sites), transitional semideciduous forests, which are semideciduous or ecotonal to Cerrado along the south-southeast margin of the Amazon (RJA, BAN sites), and Cerrado (savanna; PDG site), the southernmost site which is not within the Amazon basin (Fig. 1). The duration and strength of the dry season (defined as months where  $P < 100$  mm) varied from short and moderate at the K34 evergreen tropical forest site to long and/or intense at the PDG Cerrado and BAN ecotonal sites (Table 1 and Fig. 1). In this paper, “equatorial forest” is not intended to be representative of Amazonian equatorial forests in general, since the sites presented occur mostly on highly weathered, relatively nutrient-poor soils, in contrast to western Amazonia where soils are shallow and more nutrient-rich which support forests with higher rates of vegetation productivity and turnover (Quesada et al., 2012). Our use of the term “transitional forest” differs somewhat from other studies (e.g., da Rocha et al. (2002, 2009)), as it includes both the semideciduous forest RJA site which is proximal to but not within the forest-Cerrado ecotone and the seasonally flooded BAN site which is within the forest-Cerrado ecotone and contains both cerrado (tall ~18-m trees) and cerrado sensu stricto (closed canopy of small 5 m-tall trees interspersed with taller 7–10 m trees). The tower at the PDG Cerrado site is situated within a zone of cerrado

sensu stricto (da Rocha et al., 2002, 2009). For additional site characteristics and ecosystem behavior, see Restrepo-Coupe et al. (2013) and references therein and da Rocha et al. (2002, 2009).

Table 1 also lists the temporal coverage and frequency of the climate measurements, eddy covariance data, and ancillary soil moisture data which are available at each site, in addition to the installation depths of soil moisture sensors. All eddy covariance data have been processed according to a common protocol and are aggregated to an hourly timestep (Restrepo-Coupe et al., 2013). Soil moisture datasets were assimilated from various sources (see Table 1). The soil moisture data collection frequency ranged from near-continuous (half-hourly) to monthly and the monitored depths were variable across sites (data processing described in section 24 below and Appendix B in the Supplement).

### 2.2. Ecosystem model overview and selection

We used three to four years of climate measurements of short and long wave radiation, precipitation, air temperature, atmospheric pressure, humidity and horizontal wind speed to drive a suite of ecosystem models (23 variants in total) at each of the six sites according to a common spinup and initialization protocol. Participating models were part of the Large Scale Biosphere–Atmosphere Experiment in Amazonia Data Model Intercomparison Project (LBA-DMIP; de Gonçalves et al., 2013). All models simulated ecosystem-level evapotranspiration ( $E$ ) but used varying degrees of complexity for representing water supply and vegetation demand. 21 of the 23 model variants simulated a soil moisture store upon which vegetation draws for transpiration, but differed in the vertical resolution and depth of soil layers simulated (spanning 1.5–15 m), as well as the rooting depth used across sites. In most models, soil depth is synonymous with rooting depth. Five additional models simulated a groundwater store (also referred to as an unconfined aquifer) which could exchange water with the soil (both into and out). Table A2 in the supplementary information contains information on the models’ soil depth, pedotransfer model and bottom boundary condition, in addition to the number of soil layers and rooting depths used across sites, and the associated model reference. On the demand side, 21 of the 23 model variants simulated canopy stomatal conductance ( $g_s$ ), using one of four principal schemes to solve for  $g_s$ ,  $E$ , and leaf-level photosynthesis (if simulated) given ambient incoming radiation, air temperature, and humidity: Jarvis-type (Jarvis, 1976) (four model variants), Leuning-type (Leuning et al., 1995) (four model variants), Ball-Woodrow-Berry-Collatz (Ball et al., 1987; Collatz et al., 1991) (11 model variants), or a constant ratio of internal to external leaf  $CO_2$  concentration (2 model variants). Table A3 in the supplementary information gives the stomatal closure equations and parameter values for each model, and the associated model reference. For further information on details of model spinup and initialization procedures, see de Gonçalves et al. (2013) and references therein. Further documentation on the models analyzed here can be found in Balsamo et al. (2009), Best et al. (2011), Clapp and Hornberger (1978), Clark et al. (2011), Cox et al. (1998), de Rosnay and Polcher (1998), Ducoudre et al. (1993), Foley et al. (1996), Gerten et al. (2004), Haxeltine and Prentice (1996), Jacobs (1994), Krinner et al. (2005), Medvigy et al. (2009), Monteith (1995), Niu et al. (2011), Oleson et al. (2010), Running and Coughlan (1988), Schaefer et al. (2008), Sellers et al. (1996), Van den Hurk et al. (2000), Verseghy (1991) and Zhan et al. (2003).

### 2.3. Atmospheric and vegetation controls on $E$

We conducted a first-order assessment of the realism of mechanisms regulating  $E$  in the models by comparing the degree to which energy available to evaporate water controlled  $E$ , in models

**Table 1**  
Site characteristics, observational data descriptions and their associated references Site characteristics are from Restrepo-Coupe et al. (2013) + references therein and de Gonçalves et al. (2013) + references therein, unless otherwise noted. Dry season defined as months where precipitation is less than 100 mm.

Site lat/lon	Biome type	Group <sup>b</sup>	Site characteristics						Eddy flux measurements			Soil moisture measurements			
			Canopy height [m]	Precip [mm y <sup>-1</sup> ]	Dry season length <sup>d</sup> [months]	Dry season precip <sup>d</sup> [mm month <sup>-1</sup> ]	Soil texture <sup>e</sup>	Soil depth [m]	Years used	Freq	Tower height [m]	Years used	Freq	Measurement depths [m]	Extrap depth <sup>j</sup> [m]
K34 2.61S/ 60.21W	Tropical evergreen forest	Equatorial forest	30–35	2328	2.8	64	clay	> 15	2002–2005	Hourly	50	1992–1993 <sup>f</sup>	Weekly <sup>f</sup>	0.1, then intervals of 0.2 from 0.2 to 36 <sup>f</sup>	10.0
K67 2.85S/ 54.97W	Tropical evergreen forest	Equatorial forest	35–40	1597	6.3	49	clay	> 12	2002–2004	Hourly	63	1999–2005 <sup>g</sup>	Monthly <sup>g</sup>	0.3, 0.5, then intervals of 10 from 10 to 11 <sup>g</sup>	250
K83 3.01S/ 54.58W	Selectively logged tropical evergreen forest	Equatorial forest	35–40	1659	5.0	45	clay	> 12	2001–2003	Hourly	64	2002–2003 <sup>h</sup>	Half-hourly <sup>h</sup>	0.15, 0.30, 0.60, 10, 20, 30, 40, 60, 10 <sup>h</sup>	30.0
BAN (or JAV) 9.82S/ 50.13W	Seasonally flooded forest-savanna ecotone	Transitional forest	5–18 <sup>a,c</sup>	1680	5.3	27	clay loam	> 3	2004–2006	Hourly	40	2004–2005 <sup>c</sup>	Half-hourly <sup>c</sup>	0.1, 0.2, 0.5, 10, 15, 20 <sup>c</sup>	10.0
RJA 10.08S/ 61.93W	Tropical semideciduous forest	Transitional forest	30	2342	4.3	36	loamy sand	12–4.0	2000–2002	Hourly	60	1992–1993 <sup>f</sup>	Weekly <sup>f</sup>	0.1, then intervals of 0.2 from 0.2 to 36 <sup>f</sup>	–
PDG (or PEG) 21.62S/ 47.63W	Cerrado sensu stricto <sup>a</sup>	Cerrado	5–10	1284	7.0	40	loamy sand	1.0–3.5	2001–2003	Hourly	21	2001–2003 <sup>i</sup>	Half-hourly <sup>i</sup>	0.1, 0.2, 0.5, 0.8, 10, 15, 20, 25 <sup>i</sup>	–

<sup>a</sup> da Rocha et al. (2002, 2009).

<sup>b</sup> This study; see Section 2.

<sup>c</sup> Borma et al. (2009).

<sup>d</sup> Calculated based on time period listed in ‘Years used’ from the eddy flux measurements.

<sup>e</sup> USDA texture classification using % sand, % silt, % clay values reported in de Gonçalves et al. (2013).

<sup>f</sup> Hodnett et al. (1995).

<sup>g</sup> Nepstad et al. (2002).

<sup>h</sup> Bruno et al. (2006).

<sup>i</sup> da Rocha et al. (2002), and unpublished data.

<sup>j</sup> This study; the depth to which variations in soil moisture were extrapolated below the deepest soil moisture sensor See Section 24 and Appendix B of the Supplement for details.

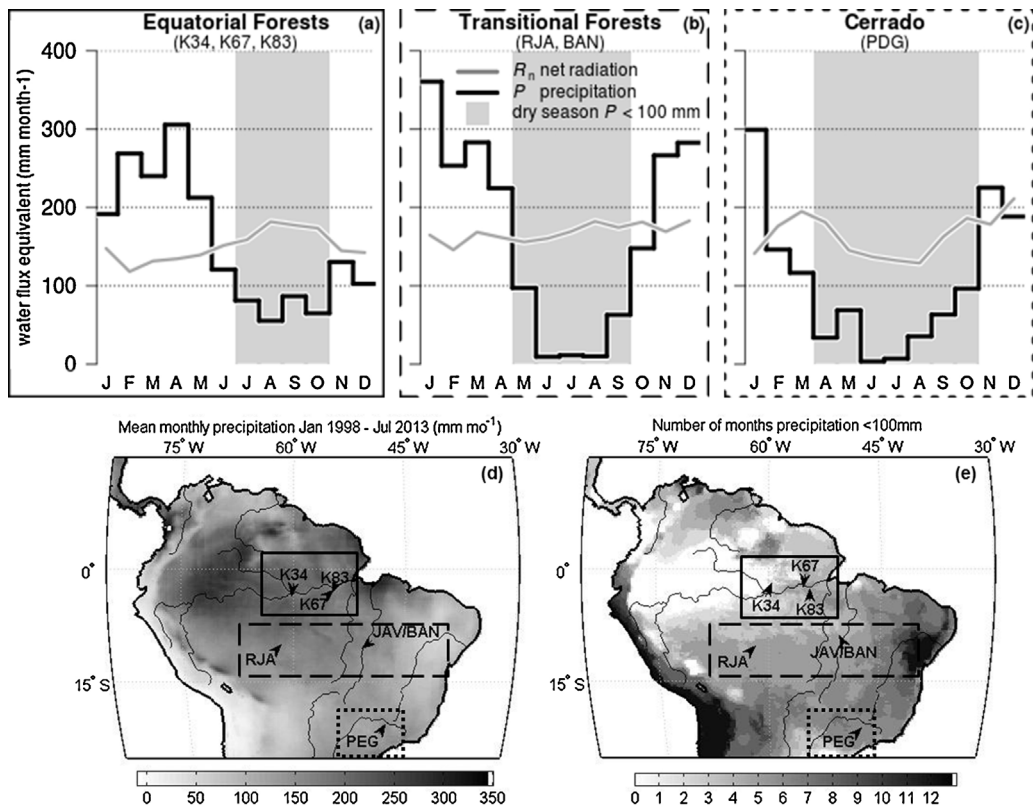


**Fig. 1.** Mean seasonal climatology (precipitation;  $P$ , net radiation;  $R_n$ , and evapotranspiration;  $E$ ) in equivalent water flux units ( $\text{mm month}^{-1}$ ) based on pooled monthly time series data from multiple sites grouped by (a) equatorial forests (K34, K67, K83 sites), (b) transitional forests (RJA, BAN sites), and (c) Cerrado (PDG site). Maps display (d) mean monthly precipitation ( $\text{mm month}^{-1}$ ) or (e) number of dry season months. Boxes around grouped sites match those around corresponding water flux figures.

versus in observations, during the dry season (defined as months where  $P < 100$  mm). We quantified this control by regressing (for both models and observations) daily mean  $LE$  ( $\text{W m}^{-2}$ ) on incoming energy and extracting the slope and  $R^2$  values. The slope indicates the relative partitioning of available energy between  $LE$  and  $H$  (higher slopes mean more  $LE$ , i.e., a lower Bowen ratio,  $\beta = H/LE$ ), while values of  $R^2$  indicate the degree to which variability in available energy drives  $LE$ , as opposed to other variables (e.g., vapor pressure deficit, aerodynamic conductance, or soil water stress).  $R^2$  values closer to 1 indicate that a large fraction of variation in  $LE$  can be explained by variation in available energy. We applied this approach uniformly across both simulations and eddy flux observations, pooling the data across sites by each site grouping (single site PDG in the case of Cerrado). We interpreted consistency between model-derived and observation-derived  $R^2$  and slope values as one metric of realism of modeled controls on  $E$ .

For these regressions, we approximated available energy with the sum of latent and sensible heat ( $LE + H$ ). Using  $LE + H$  as an estimate of available energy instead of  $R_n$  is an approach recently adopted by a pan-tropical review of  $LE$  (Fisher et al., 2009) as an alternative to filtering out periods of poor energy budget closure (periods when  $LE + H$  fall short of net radiation,  $R_n$ ), which can reduce the number of daily replicates comprising a monthly mean (Costa et al., 2010). We recognize that such an approach inflates  $R^2$  values and increases the slope, but absolute values are not the emphasis here. Rather, we sought a means by which to assess site-site and model-data differences in the responses of  $LE$  to available energy in a way that was not confounded by varying degrees of energy budget closure in the observations. This allowed us to eliminate the possibility that differences in regression slopes or  $R^2$  values across sites or between models and observations were due to the energy budget closure problem (since some sites' closure is better than others and all models have near-perfect closure).

#### 2.4. Supply-side analysis of the seasonality of $E$ : coupling with soil moisture measurements

All models presented were verified to have balanced the water budget; i.e., the following equation was always satisfied (de Gonçalves et al., 2013) to within  $5 \text{ mm month}^{-1}$ .

$$P - E - Q_s - Q_{sb} + Q_{g\uparrow} = \frac{\Delta S_i + \Delta S_o + \Delta S_s}{\Delta t} \quad (1)$$

where the left-hand side represents the net water flux into the system in units of  $\text{mm month}^{-1}$  and the right hand side is the month-to-month differenced water storage of the system ( $\Delta t$  in months).  $P$  is the precipitation,  $E$  the total evapotranspiration,  $Q_s$  the surface runoff,  $Q_{sb}$  the subsurface drainage,  $Q_{g\uparrow}$  the vertical or lateral recharge to the soil from groundwater (positive from groundwater to unsaturated soil),  $\Delta S_i$  the change in canopy intercepted water,  $\Delta S_o$  the change in ponded surface open water, and  $\Delta S_s$  is the change in total soil moisture. At the monthly timescale,  $\Delta S_i$  and  $\Delta S_o$  for all models were comparatively much smaller than  $\Delta S_s$ .

We used a water budget approach to analyze supply-side mechanisms governing the seasonality of  $E$ . We combined precipitation and estimates of  $E$  with ancillary soil moisture measurements to estimate (as a residual) the seasonality of total runoff and groundwater recharge. This gave us all of the major components of the water budget for each site, and allowed us to infer the relative roles of upward capillary flux from groundwater and deep root uptake in sustaining dry season rates of  $E$ . These two mechanisms differentially impact both the magnitude and timing of the variability in total soil moisture; thus, quantifying the variability of and timing of changes in  $\Delta S_s$  provides a means for validating model mechanisms of water supply.

We used seasonal cycle estimates of  $E$  and month–month changes in stored soil moisture ( $\Delta S_s$ ), together with the seasonal cycle of precipitation ( $P$ ) to estimate the seasonal cycle of total runoff ( $Q_t$ ; positive means loss from the ecosystem), assuming a simple water balance model:

$$Q_t = P - E - \Delta S_s \quad (2)$$

We additionally assumed that month-to-month changes in stored canopy intercepted water were negligible. While we are unable to discriminate the partitioning of  $Q_t$  between surface runoff ( $Q_s$ ) and subsurface drainage ( $Q_{sb}$ ), we note that any  $Q_t$  occurring in the dry season will be dominated by subsurface drainage because surface soils are unsaturated. Most importantly, this approach also allows us to estimate the role of upward capillary flux or lateral transport from groundwater ( $Q_{g\uparrow}$ ) during the dry season (inferred whenever  $Q_t < 0$ , or in other words, when the rate of soil moisture depletion is less than the rate of accumulating water deficit) as a mechanism for buffering dry season water deficits.

The seasonal cycle of  $P$  was estimated from the precipitation driver data, which was site-derived (de Gonçalves et al., 2013). We estimated the seasonal cycle of  $E$  from hourly eddy covariance turbulent flux measurements by first making daily estimates from daylight hours, followed by monthly  $E$  totals, and then averaging across years. Days with less than 80% data availability (Hasler and Avissar, 2007) and months with insufficient data for computing at least 7 daily totals were excluded. To derive modeled seasonal cycles of  $E$ , we used the entire model output, having determined that the seasonality of modeled  $E$  was not significantly impacted by removing model output hours during nighttime or periods of unavailable eddy flux observations of  $E$ .

To estimate the seasonal cycle of  $\Delta S_s$ , we assimilated datasets of soil moisture measurements from various sources (Table 1). We estimated the month-to-month changes in total soil moisture ( $\Delta S_s$ ) by aggregating to monthly means, integrating over depth, time differencing the monthly means, followed by averaging over replicate years. Where possible, we estimated the contribution to total  $\Delta S_s$  of soil moisture below the measured domain (see Appendix B for methods), and found that at most sites and months, it was small (Supplement Fig B4). The  $Q_{g\uparrow}$  reported in Fig. 4 accounts for the additional variation in soil moisture beyond the measured depth up to the extrapolated depth reported in Table 1 for each site, except where extrapolation was not possible (PDG).

## 2.5. Demand-side analysis of the magnitude and seasonality of $E$

To provide a more rigorous assessment of the degree of potential dry season limitation of  $E$  by vegetation, we estimated seasonal variability in stand-level canopy stomatal conductance ( $g_s$ ), using a top-down approach, similar to the inverted Penman-Monteith equation, but one which more closely approximates canopy stomatal conductance (as opposed to surface conductance) (Baldocchi et al., 1991). We applied the same top-down approach to extract canopy stomatal conductance from the models with hourly output (rather than using simulated canopy conductance directly) to make data-model intercomparison more straightforward. Models with daily output were excluded from these analyses because of the difficulty in estimating  $g_s$  from daily means. Exceptions are SiB3, SiBCASA and LEAFHYDRO models, which simulate a prognostic air space; canopy conductance from SiB3 and SiBCASA model output was used directly in lieu of the method described below.

The approach for estimating  $g_s$  is as follows: First, we estimated aerodynamic boundary layer resistance  $r_b$  ( $s\ m^{-1}$ ):

$$r_b = \frac{\bar{u}}{u_*^2} \quad (3)$$

where  $\bar{u}$  is the horizontal wind speed ( $m\ s^{-1}$ ) and  $u_*$  is the friction velocity ( $m\ s^{-1}$ ). Eq. (3) follows Costa et al. (2010) and Hasler and Avissar (2007) who used it to estimate  $r_b$  (or its inverse) at sites in central and southern Amazonia, many of which are the same sites reported here. While  $r_b$  can also be a function of measurement height, surface roughness and atmospheric stability, we kept a simple formulation based on the first-order  $\bar{u}/u_*^2$  term because this avoids potential errors associated with second-order stability terms (Costa et al., 2010). We expect the biggest impact of not accounting for these higher order terms to be in the magnitude of  $r_b$  estimated across sites, and so we focus on cross-site differences in the seasonality  $g_s$  (which depends on  $r_b$ ; see Eq. (5) below), as opposed to its magnitude. We are still able, however, to compare the magnitude of  $g_s$  between models and data within a given site because we apply the same approach to estimate  $r_b$  and  $g_s$  in models and observations.

We then use  $r_b$  coupled with eddy covariance estimates of sensible heat flux ( $H$ ;  $W\ m^{-2}$ ) to estimate an aerodynamic canopy temperature  $T_v$  ( $^{\circ}C$ ) by rearranging the gradient approximation for sensible heat flux ( $H$ ):

$$T_v = \frac{r_b H}{c_p \rho_a} + T_a \quad (4)$$

where  $c_p$  is the specific heat capacity of dry air ( $J\ kg^{-1}$ ),  $\rho_a$  the atmospheric air density ( $kg\ m^{-3}$ ), and  $T_a$  ( $^{\circ}C$ ) is the atmospheric air temperature measured at the tower top  $T_v$  is not necessarily leaf temperature, though the two are related. It is best understood as the temperature of the leaves and branches which contribute most to aerodynamic drag. Concurrent measurements of leaf temperature and an eddy covariance-estimated  $T_v$  at the K83 site show that the two are temporally correlated with each other but individual leaf temperatures can exceed  $T_v$  by as much as  $8^{\circ}C$  under sunny conditions (Doughty and Goulden, 2008). Once  $T_v$  is known, we can estimate canopy stomatal conductance (Baldocchi et al., 1991):

$$g_s = \left[ \frac{\rho_a (q_{sat}(T_v) - q_a)}{E_t} - r_b \right]^{-1} \quad (5)$$

where  $q_{sat}(T_v)$  is the saturation specific humidity ( $kg\ kg^{-1}$ ) at vegetation temperature  $T_v$  and  $q_a$  is the ambient specific humidity ( $kg\ kg^{-1}$ ), and  $E_t$  is the transpiration rate ( $kg\ m^{-2}\ s^{-1}$ ).

We estimated  $E_t$  on a site-by-site basis as follows. First, we identified time periods when canopy interception evaporation ( $E_i$ ) was nonzero as predicted by the CLM3.5 model. Then, assuming that these periods were a good proxy for times when the canopy was wet, we removed these same periods from the  $E$  dataset prior to any averaging. For consistency, we applied this same method on all models to estimate  $E_t$  from the models'  $E$  output (as opposed to using the models'  $E_t$  output directly). While imperfect, this method ensured that  $E_t$  in observations and models came from periods of identical environmental forcing. The method used to estimate  $E_t$  is only suitable for analyzing its seasonality and relative magnitude across models and observations, but not its absolute magnitude. This is because the method does not equally sample the net radiation distribution, due to a bias towards cloud-free periods arising from the need to exclude periods when the canopy was wet. For this reason, we did not attempt to estimate the transpiration fraction of evapotranspiration, though it is likely a large fraction for the forest sites (Jasechko et al., 2013).

The slope of leaf-level stomatal conductance versus photosynthesis is the parameter  $m$  in the Ball–Woodrow–Berry–Collatz (BWBC) semi-empirical model of stomatal conductance (Collatz et al., 1991) (see Table A3), the inverse of which we refer to as intrinsic water use efficiency of photosynthesis ( $iWUE$ ), following the definition of Beer et al. (2009). Even though not all models use the BWBC model, we could estimate  $m$  and  $iWUE$  at the canopy scale

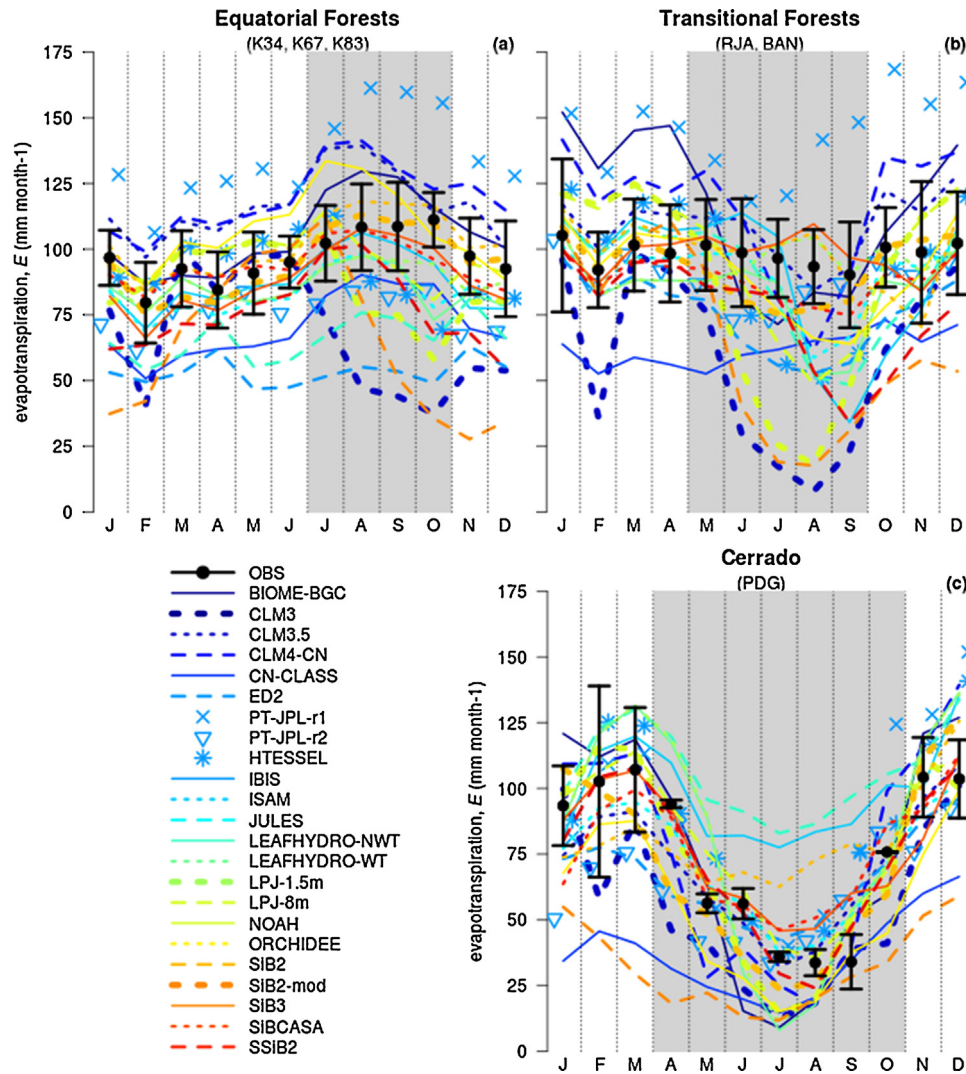


**Fig. 2.** Modeled (colored lines or symbols) and observed (black points and error bars) mean seasonal cycle of  $E$  based on monthly time series data averaged ( $\pm 1$  standard deviation) across multiple sites grouped by (a) equatorial forest (K34, K67, K83), (b) transitional forest (RJA and BAN) and (c) Cerrado/savanna (PDG). For (a) and (b), error bars incorporate inter-site and interannual variability, whereas for (c), error bars represent interannual variability only. Gray shaded region denotes dry season (months where precipitation < 100 mm).

for those which simulate  $GPP$  in addition to  $E$ . We estimated  $m$  as the slope of the best fit line between  $g_s$  and  $GPP_{norm} = GPP \times (h/c_a)$  and took  $iWUE = 1/m$ , where  $c_a$  and  $h$  are ambient  $CO_2$  mole fraction and relative humidity, respectively. Because the intercept of this relationship across the majority of models and observations was near zero, we forced all fits through the origin. While the flux tower observations were nearly linear, many models were slightly non-linear at high levels of  $GPP_{norm}$  and were also affected by outliers in  $g_s$ . We dealt with this issue by fitting models with a 2nd degree polynomial through the lower quantile of  $g_s$  (as opposed to the mean of  $g_s$  which would have been affected by outliers) and estimated the slope at an intermediate value of  $GPP_{norm} = 30 \times 10^4 \mu mol m^{-2} s^{-1}$  where the fitted polynomial was approximately linear. We estimated the uncertainty about observed  $iWUE$  as the inverse of the upper and lower quartile fits of  $m \sim GPP_{norm}$  and uncertainty in  $GPP$  as the pooled standard deviation about the daily mean (across days and years). With estimates of  $iWUE$  and  $GPP_{norm}$ , we were able to address the degree to which some of the spread in the simulated magnitude of  $E$  across models could be related to compensating errors in these variables which regulate vegetation demand for water.

### 2.6. Site and model representation in analyses

Sites were represented in analyses as follows. For the first-order analysis of the seasonality of  $E$  (Fig. 2) and its control by available energy (Fig. 3), we sought to show how the sites behaved in accord to their site grouping along the north-south gradient of climate and vegetation. In these figures, we present the observed and modeled data either averaged (Fig. 2) or pooled (Fig. 3) within each site grouping. In analyses of supply (Fig. 4) and demand (Figs. 5–7), a site-specific approach was more appropriate because we were adjoining ancillary soil moisture data or momentum and carbon fluxes to the water flux data. In these figures, we selected one site to represent each of the three site groups. We selected K67 to represent the equatorial forests since this site had the best data quality and coverage and because model-model differences were most apparent at this site compared to K34 and K83. We selected the seasonally flooded BAN site for the transitional forests in analyses of water supply because this site behaved most differently when compared to the equatorial forest and Cerrado sites. However, mechanisms of water supply at the BAN site should not be interpreted to be characteristic of RJA or transitional forest sites in

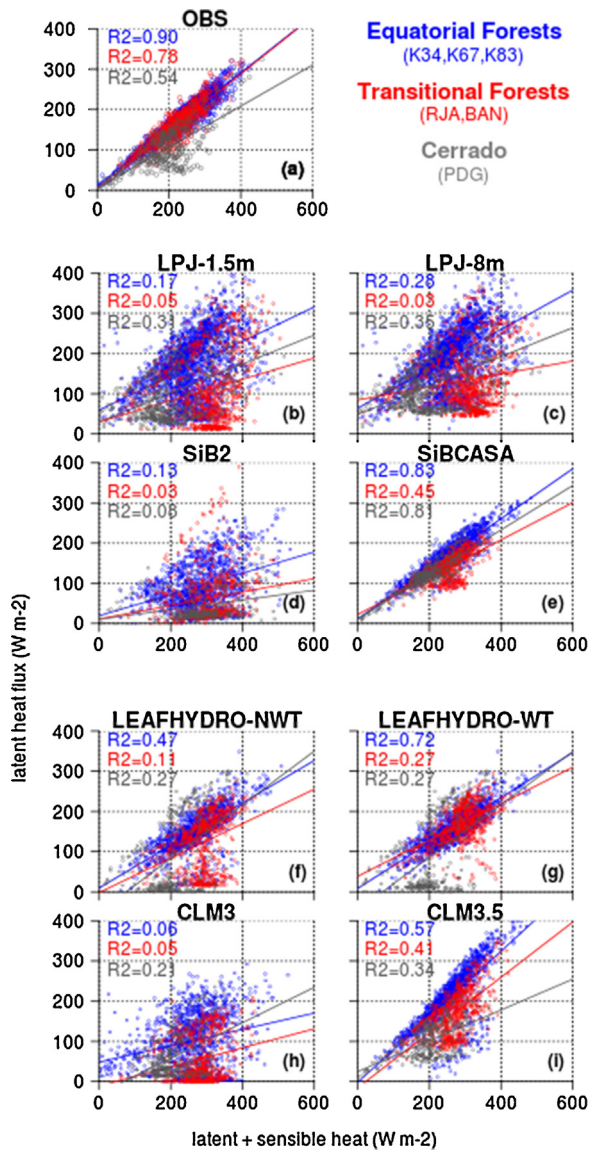


**Fig. 3.** Scatterplots and least squares linear regression of daily values of dry season  $LE$  versus  $LE+H$  for (a) observations and (b)–(i) select models (see main text for model selection criteria and justification of choice of  $LE+H$  as  $x$ -axis variable). Deep roots are implemented in the model developments from (b)  $\rightarrow$  (c) and (d)  $\rightarrow$  (e); groundwater is implemented in model developments from (f)  $\rightarrow$  (g) and (h)  $\rightarrow$  (i). Data for equatorial and transitional forests were pooled, not averaged, across sites.

general. We used the RJA site to represent transitional forest sites in the analyses of demand, since the assumption of negligible soil evaporation at BAN is invalid. As the PDG site was the only Cerrado site, it is displayed in all analyses to represent the Cerrado group.

Models were represented in analyses as follows. For the correlation analysis of evapotranspiration with available energy (Fig. 3) and the analysis involving the mechanisms of supply (Fig. 4), we chose a subset of models which had added or changed different mechanisms hypothesized important for regulating the seasonality of  $E$ , and evaluated the effectiveness of these changes in improving subsequent model performance. These changes in structure fell into two main groups: (1) increases in soil and rooting depth beyond 3.5 m, and (2) addition of a groundwater reservoir which was allowed to exchange water with unsaturated soil (as opposed to a standard free drainage bottom boundary condition). Within each of these two groups, we selected two models with versions prior to and following the associated structural change and the two models within each group were selected to illustrate the range

of sensitivity to the structural change. This gave us a total of four unique “model families” and eight discrete model simulations on which we focused for the three sites. We selected the LPJ and SiB model families (LPJ-15 m, LPJ-8 m, SiB2, and SiB3 or SiBCASA) to illustrate the effect of implementing deep roots since the effect of adding deep roots was weakest in LPJ and strongest in SiB3 and SiBCASA. We selected the CLM and LEAF model families to illustrate the effect of adding interaction with groundwater since the strength of the effect for these models was different at different sites. Collectively, these models spanned the range of performance with respect to the observed seasonality of  $E$  (Fig. 2).

In the analysis of the mechanisms of vegetation demand, we first chose a subset of models at each of three different sites which simulated well the seasonality of observed  $E$  (SiB3, IBIS, JULES and ORCHIDEE at K67; SiBCASA, NOAH, LEAFHYDRO-WT and SiB3 at RJA; CLM35, ISAM, SiB3, SiBCASA and SSiB2 at PDG), in order to assess whether or not these models did so while also capturing the seasonality of canopy stomatal conductance ( $g_s$ ). We then selected all models which simulated both carbon and water fluxes, except models which were run on a daily timestep (see Section 25), to assess how the combined  $g_s$  and intrinsic water use efficiency of photosynthesis ( $iWUE$ ) mechanisms impacted the magnitude of modeled  $E$  (Fig. 7).

### 3. Results and discussion

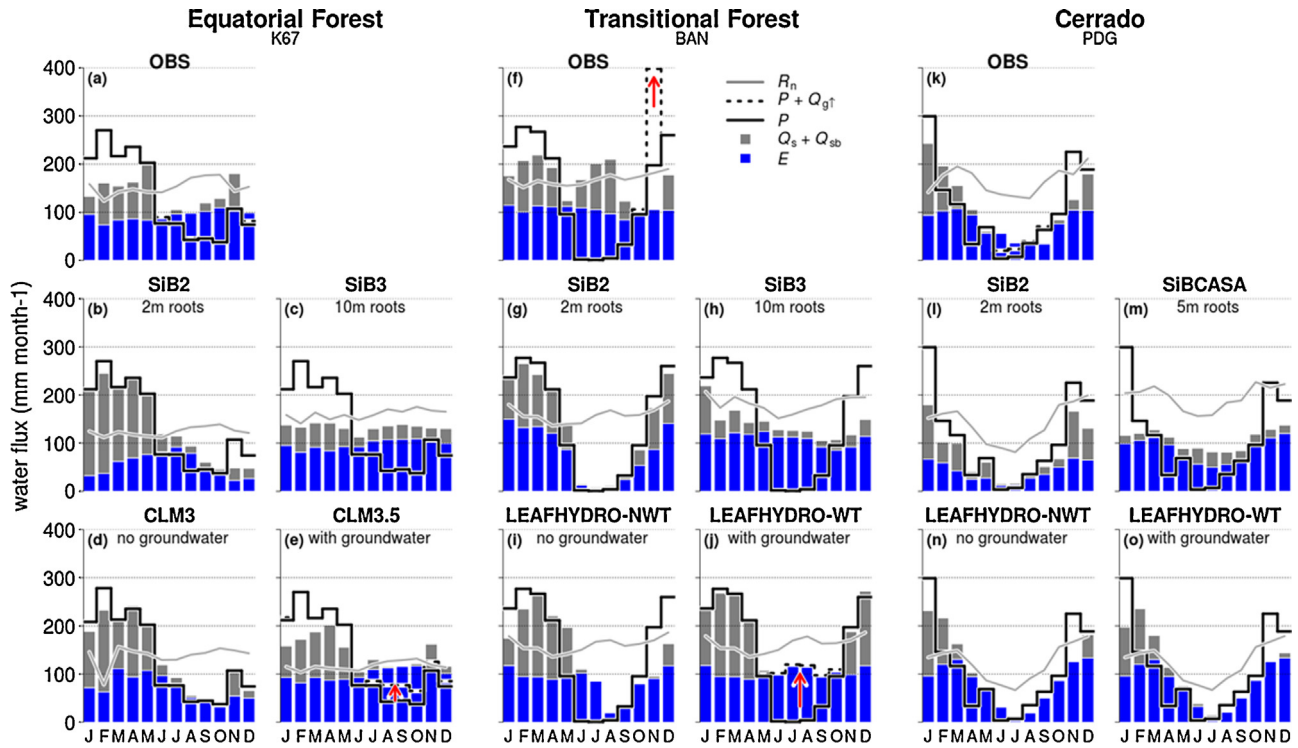
#### 3.1. Seasonal cycles of $E$ across sites

Fig. 2 shows that equatorial forests exhibit a seasonal cycle of  $E$  peaking with net radiation during the dry season, transitional southern forests show either a flat seasonal cycle (due to less seasonality in available light) or a slight dry season depression (some degree of water limitation), and Cerrado demonstrates a strong dry season depression (both due to reductions in light and water). These results corroborate those of previous work which showed a general trend of increasing water limitation from north to south (Hasler and Avissar, 2007; Juarez et al., 2007; Borma et al., 2009; da Rocha et al., 2002, 2009; Fisher et al., 2009). While BAN and RJA differed slightly in their respective seasonalities of  $E$  (BAN has a more pronounced dry season depression compared to RJA), overall the individual site  $E$  seasonalities corresponded to the mean  $E$  seasonality of the grouped sites (see Appendix D of the supplement for individual site seasonalities).

Models in general performed best at the end members of the precipitation gradient (Fig. 2a and c) but more poorly at transitional forest sites (Fig. 2b). In particular, models performed best at equatorial evergreen sites, with 13 and 15 out of 23 models capturing the observed magnitude and seasonality, respectively, of the mean  $E$  across these sites (Fig. 2a). Models comparatively performed most poorly at transitional forest sites (Fig. 2b) and to an intermediate degree at Cerrado (Fig. 2c).

#### 3.2. Available energy as a driver of $E$

Cerrado demonstrated a clear contrast to equatorial and transitional forests in terms of how available energy controlled dry season  $LE$ , demonstrated by a significantly smaller slope of  $0.51 \pm 0.03$  (95% confidence interval) and coefficient of determination ( $R^2$ ) value of 0.54 (Fig. 3 and Table 2). In other words, available energy during the dry season heats vegetation more in Cerrado compared to forests, and Cerrado vegetation is also less responsive to variations in available energy. The equatorial and transitional forests exhibited nearly the same partitioning between  $LE$  and  $H$  during the dry season with slopes of  $0.70 \pm 0.01$  and  $0.71 \pm 0.01$ , respectively (95% confidence intervals), but environmental factors



**Fig. 4.** Observed (top row) and modeled (bottom two rows) monthly averages of the seasonality of net radiation ( $R_n$ ), precipitation ( $P$ ), evapotranspiration ( $E$ ), total runoff ( $Q_s + Q_{sb}$ ), and the influx of groundwater ( $Q_{g†}$ ) for three sites. Soil moisture storage (positive) or depletion (negative) is given by the difference between the top of largest of the two lines ( $P$  or  $P + Q_{g†}$ ) and the top of the stacked bars. Contrasting predictions due to shallow vs deep roots are shown in the middle row; contrasting predictions due to absence vs presence of groundwater interaction are in the bottom row. Red upward arrow denotes influx of groundwater into the system.

other than available energy are apparently more involved in controlling variation in  $LE$  in transitional forests, evidenced by a lower  $R^2$  value of 0.78 compared to 0.90 for equatorial forests (Table 2). In sum, the fraction of total variance in  $LE$  explained by available energy during the dry season moderately decreased with increasing strength of the dry season, presumably due to increasing degrees of dry season humidity or water deficits. Again, we emphasize relative differences in slopes and  $R^2$  values across sites as opposed to absolute values. High dry season  $R^2$  values at equatorial sites, however, did not preclude the role of vegetation demand (see Section 34).

For most models with shallow soil (LPJ-15 m, SiB2, CLM3; all with soil depths <3.5 m), available energy explained little of the total variance in  $LE$  in these models at all sites ( $R^2 < 0.31$ ) (Fig. 2 and Table 2). The exception to this was LEAFHYDRO-NWT, which had much higher  $R^2$  at equatorial sites but a low bias in its regression slope. When the shallow soil models were modified to have either deep soil or interaction with groundwater, they significantly improved dry season  $LE$  via increases in  $R^2$  and slope, except for LPJ.

Low infiltration capacity and high rates of surface runoff apparently limited the water available to deep soil and roots for sustaining  $LE$  during the dry season in this model (see Appendix D of the Supplement). For other models, fixing the supply side of the water limitation problem revealed significant positive biases in the partitioning of  $LE$  relative to  $H$  under non-water stressed conditions, evidenced by slopes exceeding those of the observations. At Cerrado, SiBCASA had a slope of  $0.55 \pm 0.02$  (not significantly greater than the observations) and at the equatorial forest sites CLM3.5 had a slope of  $0.82 \pm 0.02$ , significantly greater than the observations ( $0.70 \pm 0.01$ ) (Table 2; see also ED2, JULES, IBIS at Cerrado in Appendix C of the Supplement). Thus, it was not uncommon for models to “overfix”  $E$  when eliminating water limitation.

### 3.3. Supply-side mechanisms of E

Overall, models with soil depths less than or equal to 3.5 m and without groundwater interaction were not able to simulate

**Table 2**

Summary statistics (intercepts, slopes, coefficient of determination  $R^2$ ) for the linear regressions shown in Fig. 3 of latent heat flux ( $LE$ ) on  $LE$  + sensible heat flux ( $H$ ) as observed (in bold) and modeled for the three site groups. Eq, Equatorial forest sites; Tr, transitional forest sites; Cr, Cerrado site. The slopes of all regressions listed are significantly different from zero ( $p < 0.001$ ).

Observations or model	Intercept			Slope			$R^2$		
	Eq	Tr	Cr	Eq	Tr	Cr	Eq	Tr	Cr
<b>Observations</b>	<b>11</b>	<b>4</b>	<b>5</b>	<b>0.70</b>	<b>0.71</b>	<b>0.51</b>	<b>0.90</b>	<b>0.78</b>	<b>0.54</b>
LPJ-15 m	59	30	30	0.43	0.26	0.36	0.17	0.05	0.31
LPJ-8 m	64	85	49	0.49	0.16	0.36	0.28	0.03	0.35
SiB2	19	11	10	0.26	0.17	0.12	0.13	0.03	0.08
SiBCASA	12	22	12	0.62	0.46	0.55	0.83	0.45	0.81
LEAFHYDRO-NWT	10	-2	-50	0.53	0.43	0.67	0.47	0.11	0.27
LEAFHYDRO-WT	9	38	-46	0.56	0.45	0.66	0.72	0.27	0.27
CLM3	48	-11	-30	0.20	0.24	0.44	0.06	0.05	0.21
CLM35	-2	-16	25	0.82	0.69	0.38	0.57	0.41	0.34

**Table 3**  
Observed (in boldface) and modeled annual totals, monthly maxima, and the month in which the maximum occurs for the upward capillary flux of groundwater into soil ( $Q_{gt}$ ) at the three sites presented in Fig. 4. “OBS-a” and “OBS-b” refer to the inferred  $Q_{gt}$  flux occurring at the depth of the extrapolated soil moisture and the deepest soil moisture sensor, respectively (see Table 1 and Appendix B of the supplement).

Observations or model	Total (mm year <sup>-1</sup> )			Monthly maximum (mm month <sup>-1</sup> )			Month of maximum		
	BAN	K67	PDG	BAN	K67	PDG	BAN	K67	PDG
<b>OBS-a</b>	<b>211</b>	<b>24</b>	–	<b>201</b>	<b>13</b>	–	<b>Nov</b>	<b>Jun</b>	–
<b>OBS-b</b>	<b>229</b>	<b>22</b>	<b>44</b>	<b>204</b>	<b>18</b>	<b>16</b>	<b>Nov</b>	<b>Dec</b>	<b>Jun</b>
CLM35	14	137	0	14	35	0	Nov	Aug	–
CLM4CN	204	278	10	49	54	3	Aug	Oct	Nov
ISAM	0	0	11	0	0	7	–	–	Nov
LEAFHYDRO-WT	416	92	0	119	26	0	Jul	Oct	–

$E$  without a dry season depression (Fig. 4b, d, g, i, l, n; see also Appendix D of the Supplement). Addition of an unconfined aquifer (CLM3.5, LEAFHYDRO-WT models) produced a similar effect on dry season water stress as did addition of deep soil and roots (LPJ-8 m, SiB3, SiBCASA models). Increasing the soil depth or addition of an aquifer in most models decreased total runoff and increased the water storage capacity of soil (or soil-aquifer system, for models simulating one), providing a buffer for dry season deficits. In all instances, where models erroneously predict a dry season depression in  $E$ , models overestimate wet season total runoff ( $Q_s + Q_{sb}$ ) and underestimate wet season soil water storage (e.g., SiB2 and CLM3 models in Figs. 3–4). Therefore, we deem simulation of the seasonal patterns of soil moisture recharge and discharge critical to an accurate prediction of the seasonality of  $E$ . An exception to this was the LEAFHYDRO model, where addition of an aquifer was accompanied by an increase in drainage out of the soil column, but this was an artifact of a fixed water table depth in this model (seasonal water table variation in this model requires a representation of topography, and hence, was not possible with these 1D simulations) (Miguez-Macho and Fan, 2012).

At the equatorial evergreen forest site K67, SiB3 and CLM3.5 both had seasonal patterns of  $E$  that closely matched observations, but diverged in their simulated attribution of the soil water balance to seasonal patterns of soil moisture storage and runoff (Fig. 4c and e). SiB3 had large seasonal swings in stored soil moisture accompanied by a low rate of total runoff throughout the entire year, while CLM3.5 had lower seasonal variation in soil moisture, in addition to substantial dry season upward capillary flux ( $Q_{gt}$ ) from groundwater (simulated water table depth was 3.6–4.8 m in this model).

A comparison to the water budget analysis derived from the observed seasonal cycles of  $P$ ,  $E$ , and  $\Delta S_s$  provides the necessary insight to discriminate among the dry season supply-side mechanisms used in the models. We infer a negligible role for upward capillary flux from a groundwater (does not exceed 18 mm month<sup>-1</sup>) in regulating dry season  $E$  at the K67 equatorial forest site (Fig. 4a and Table 3). The observations indicated that soil moisture storage in the unsaturated rooting domain to 11 m was able to endure a cumulative ~340 mm reduction to sustain the dry season water deficit (Supplement Figure B4d). At this site, nearly all of the total runoff ( $Q_s + Q_{sb}$ ) occurs during the wet season months of January–May, with minimal drainage during the dry season months June–Oct (i.e., nearly all of the reduction in soil moisture during the dry season is due to root uptake). This stands in contrast with CLM3.5 (Fig. 4e) and other models (Supplement Fig D2) whose dry season  $E$  rates were sustained in part by capillary fluxes from below the simulated rooting zone. Absence of shallow groundwater in the Tapajós region is also corroborated by anecdotal evidence reported in the literature (reported at depths of ~100 m in Nepstad et al., 2002; Belk et al., 2007), but it is important to note that water tables this deep are not characteristic of Amazonia in general (Miguez-Macho and Fan, 2012). The observations further bound the degree

of seasonal variation in soil moisture predicted by deep-root models (e.g., variation SiB3 is too large; Fig. 4c).

The transitional forest BAN differed dramatically in its seasonal hydrology from that at K67; it has a shallow water table and floods during the wet season. Consequently, the two model approaches (deep roots and groundwater) diverged in terms of the mechanism of dry season water supply, despite similarities in their respective seasonalities of  $E$  (Fig. 4h and j). LEAFHYDRO-WT with water table dynamics (Fig. 4j) simulates seasonal changes in water storage and depletion entirely from groundwater instead of from the unsaturated rooting domain. SiB3 with deep roots (Fig. 4h), on the other hand, drew upon stored soil moisture from deep layers (to 10 m) to make up for dry season water deficits. While both models with these modifications simulate the overall seasonality of  $E$  well, the observations indicated slight reductions in  $E$  during the dry season in June through September, which were best captured by SiB3.

Surprisingly, the water budget analysis for the BAN site (Borma et al., 2009) revealed that observed seasonal patterns of soil moisture storage and groundwater flux were not consistent with either of the deep soil/deep roots or groundwater formulations (Fig. 4f, h and j). While groundwater fluxes are significant (total annual influx of 211 mm year<sup>-1</sup>), their timing (almost all during the month of November) is not such that they contribute significantly to dry season  $E$  (Table 3). Rather, stored soil moisture to 2 m depth is more than sufficient to supply the entire dry season  $E$  water deficit, evidenced by reductions in soil moisture which exceed  $E$  losses, resulting in significant total runoff ( $Q_s + Q_{sb}$ ) occurring throughout the dry season (Fig. 4f). A large influx of groundwater into the system is inferred during the month of November because soil water increases by nearly double the incoming precipitation, even when the soil moisture measurements are not extrapolated beyond the measurement domain (Table 3). The abrupt influx of groundwater ( $Q_{gt}$ ) into this system occurs not because of soil type or depth, but because of this site's proximity to a floodplain (Borma et al., 2009), and no further net influx of groundwater after November is recorded because the soil quickly becomes and remains saturated throughout the flooding period. This highlights the importance of modeling groundwater fluctuations as a 2-dimensional topographically driven process, in which orientation in relation to drainage basins makes a big difference (Fan and Miguez-Macho, 2010). On the other hand, the role of persistent deep roots regulating  $E$  at this site is likely also be limited, given the presumed anoxic soil conditions which persist during the flooding period.

At the Cerrado site PDG, we inferred a small (16 mm month<sup>-1</sup>) upward groundwater flux during the dry season months of June and July (Fig. 4k). However, this is probably an artifact and likely represents root uptake below 2.5 m. Soil moisture measurements extended to a depth of 2.5 m only at this site (Table 1) and we were unable to extrapolate variations in soil moisture beyond this depth (see Appendix B of the Supplement). We argue that the 16 mm month<sup>-1</sup> water flux during these months actually represents deep root uptake (beyond 25 m) because a large dry season

reduction in soil moisture content still occurs at 2.5 m (Supplement Fig B1) and there is no reason to believe such seasonal variability would not continue at depths beyond 2.5 m, but this needs to be tested with deeper soil moisture measurements. Regardless, this site still demonstrated a significant degree of water stress, evidenced by a substantial depression in  $E$  during the dry season, in phase with reductions in available energy ( $R_n$ ), but with a substantial fraction of variation in  $E$  left unexplained and a smaller evaporative fraction (lower  $R^2$  and slope in Fig. 3a). The SiB2 and LEAFHYDRO-NWT models underestimated dry season  $E$  in the absence of any deep rooting or groundwater mechanisms (Fig. 4l and n). Unlike what was observed at equatorial and transitional sites, however, model results at this site showed that inclusion of deep soil/roots or groundwater mechanisms did not produce similar dry season patterns in  $E$ ; only the deep roots mechanism was able to significantly increase dry season  $E$  (Fig. 4m). The model results thus suggest that deep roots indeed play an important role in maintaining dry season  $E$ . Nonetheless, the simulated magnitude of the effect that deep roots has in supplying dry season  $E$  is still often overestimated (e.g., SiBCASA Fig. 4m and JULES, IBIS Supplement Fig D6), revealing model errors with respect to vegetation demand, which we discuss in the next section.

Potential limitations in this analysis are predominantly associated with the estimation of total soil moisture from the observational data. In some cases, the period of available soil moisture observations did not exactly coincide with the flux tower observations (Table 1). However, our use of the seasonal cycle helped to mitigate this problem. Errors associated with this likely are to be concentrated at wet/dry season boundaries; but we focused our interpretation based on coarse wet versus dry season patterns, limiting the possibility of making erroneous conclusions. Furthermore, at the one site (BAN) where we infer important groundwater fluxes at the seasonal boundaries, the soil moisture observations corresponded to 2 out of the 3 years of available flux tower data (Table 1).

The second source of uncertainty associated with the use of the soil moisture data are the estimates of upward capillary flux. The method of estimating the observed water budget also makes an estimate of the contribution of an upward capillary water flux ( $Q_{g\uparrow}$ ) to dry season evapotranspiration, which in most months is a small fraction of total  $E$ . Such an upward capillary flux is inferred when the dry season water deficit ( $P-E$ ) is not matched by a corresponding reduction in root zone soil moisture. To be clear, such an estimate likely underestimates the total upward capillary flux, since it represents only that portion of the capillary flux used by evapotranspiration. Absence of inferred capillary flux also does not necessarily rule out the role of an aquifer, either. While there may be no inferred upward capillary flux (i.e., total water potential does not increase with depth), saturated soil below an unsaturated root zone should reduce the downward rate of drainage relative to that expected from free drainage (i.e., matric water potential increases with depth, thus reducing the rate at which total water potential decreases with depth).

In summary, models which simulated an aquifer tended to do so at the expense of simulating seasonal swings in root zone soil moisture, often at odds with observations. On the other hand, models using a free drainage bottom boundary condition were able to mitigate the effects of excessive dry season drainage on water stress by employing a deep soil column with deep roots to access the larger total volume of water available for uptake, without fixing the drainage problem *per se*. Thus, while accurately simulating the annual cycle of  $E$ , the net effect in these models was to overestimate seasonal variability in soil moisture by overestimating dry season subsurface drainage. Given the role of accurately simulating total runoff and soil moisture for the accurate prediction of seasonal  $E$  patterns, the deep soil/groundwater tradeoff highlights the

fact that the choice of a bottom boundary condition in LSMs is not trivial (Gulden et al., 2007). Whatever the correct bottom boundary condition may be, the associated deep drainage appears to be somewhere in between that predicted by a free drainage and a saturated bottom boundary condition (Zeng and Decker, 2009).

We conclude that the mechanisms of upward capillary flux and deep root uptake are complementary and can both sustain  $E$  during the dry season, but their relative importance is site-dependent. For example, deep soils on plateaus, such as those in the Tapajós region and throughout much of eastern Amazônia have water table depths at 10–40 m (Fan and Miguez-Macho, 2010), and also have been documented to have deep roots (Nepstad et al., 1994), though the ubiquity of a deep rooting habit across species remains unknown. In contrast, at sites like RJA (Supplement Fig D4) and BAN which either have shallower soils or are proximal to drainage basins, the functional role of deep roots is dubious, and combined moisture storage and subsurface lateral flow is more important in regulating dry season water deficits. The CLM3.5 and LEAFHYDRO-WT models were run as single-point runs, and, as noted above, LEAFHYDRO is designed to capture the two-dimensional nature of groundwater flux while CLM3.5 parameterizes the exchange of soil water with groundwater using only one dimension, in the vertical. Vertical exchange in CLM3.5 is dependent on precipitation climatology alone, while in LEAFHYDRO, lateral convergence due to horizontal gradients in both climatology and topography are considered. For BAN, however, the role of groundwater may be to contribute to storage to the unsaturated zone at the onset of the wet season (as opposed to dry season capillary flux) which may then be drawn upon the subsequent dry season. More root zone soil moisture measurements combined with estimates of  $E$  and  $P$ , as well as improved knowledge of soil hydraulic properties at other sites across Amazonia are needed to address how prominent dry season capillary fluxes are in contributing to dry season  $E$ .

### 3.4. Demand-side mechanisms of $E_t$

In Fig. 5a–c, we have shown at each of three sites the models which simulated well the seasonality and magnitude of transpiration ( $E_t$ ). The trend in seasonality of  $E_t$  for the observations goes from a dry season peak in an equatorial forest (K67) to near-flat seasonality in a transitional forest (RJA), to a dry season depression in Cerrado (PDG), similar to that of evapotranspiration ( $E$ ) (Fig. 2). In contrast, the seasonality of canopy stomatal conductance ( $g_s$ ) exhibits varying degrees of a dry season depression at all sites (Fig. 5d–f), implying that regulation of water demand by vegetation persists even in the moist equatorial forests (Costa et al., 2010). While the models captured the overall shifts across sites in the magnitude of vegetation demand (i.e.,  $g_s$ ) reasonably well (Fig. 6d–f), many of these otherwise well-performing models did not capture the appropriate seasonality of  $g_s$  (e.g., SiB3, JULES, IBIS at K67; SiB3, SiBCASA, LEAFHYDRO-WT at RJA). Additionally, some models demonstrated biases in the magnitude of  $g_s$  at individual sites (e.g., IBIS at K67, LEAFHYDRO-WT at RJA). Below we explore some potential reasons for these model errors.

While higher dry season vapor pressure deficit ( $D$ ) regulates the seasonality of  $g_s$  to a certain degree at the leaf level, leaf phenology regulates the quantity and physiological efficiency of leaves at the canopy level, and thus also may regulate the seasonality of whole ecosystem vegetation demand for water. Differences in the timing of the minimum observed  $g_s$  at K67 compared to that of other sites suggest that canopy dynamics indeed play a role. While the minimum observed  $g_s$  at RJA and PDG occurs when the dry season is most intense (Fig. 5e and f; i.e., when precipitation and  $D$  reach their respective minima and maxima), the minimum  $g_s$  at K67 occurs at the beginning of the dry season, and remains constant or slightly recovers throughout the remainder of the dry season

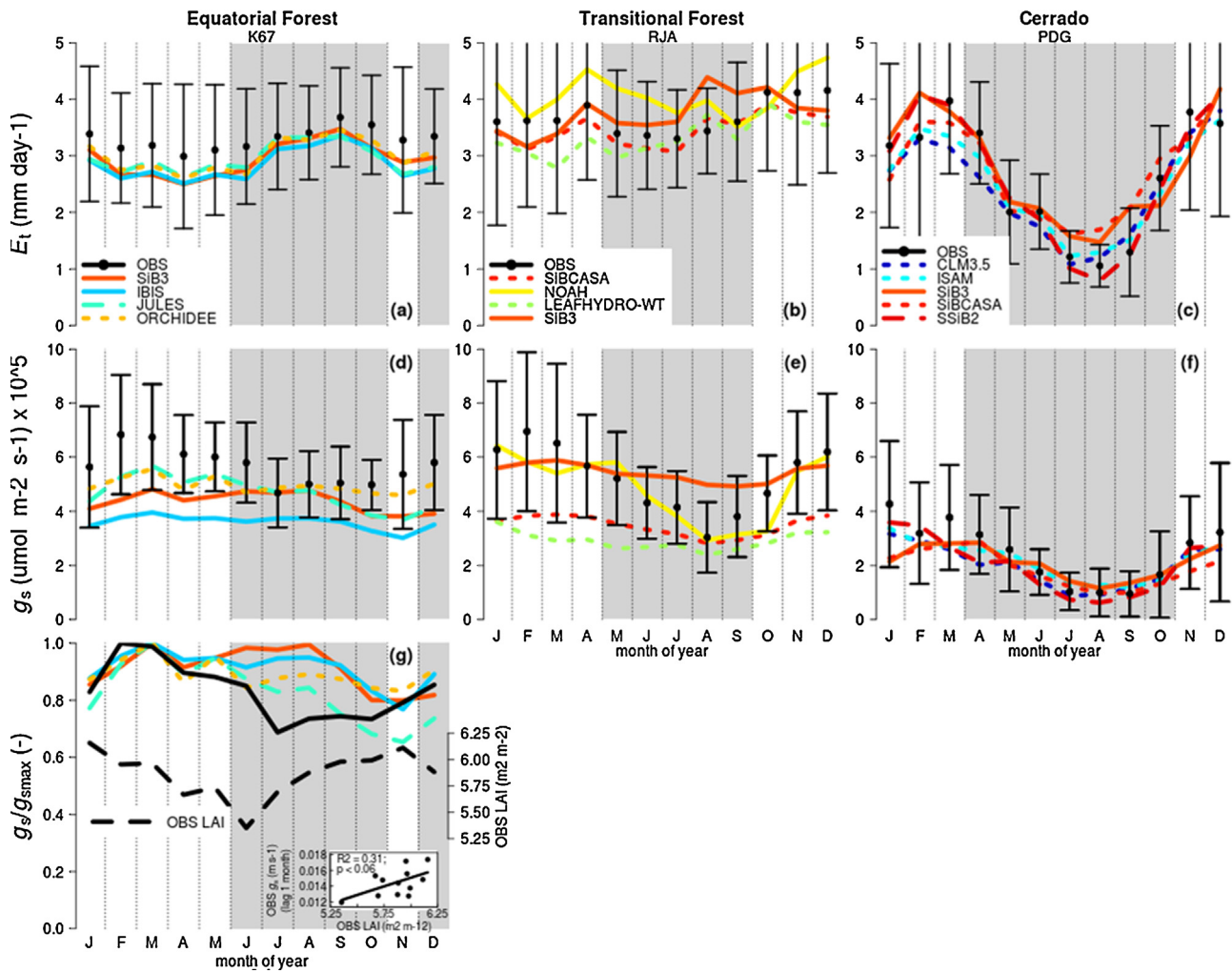


**Fig. 5.** Modeled (colored lines) and observed (points  $\pm 1$  sd) seasonal cycles of (a)–(c) transpiration ( $E_t$ ) and (d)–(f) canopy stomatal conductance ( $g_s$ ) at one site each of equatorial forests (K67), transitional forests (RJA), and Cerrado (PDG). g): Modeled (colored lines) and observed (solid black line) canopy stomatal conductance normalized by its seasonal maximum ( $g_s/g_{s\max}$ ) at the K67 site to emphasize seasonality. Inset in (g): 1-month lagged seasonal cycle of observed  $g_s$  regressed on observed LAI at the K67 site. See main text for methods of estimating  $E_t$  from eddy flux measures of  $E$ , and for estimating  $g_s$ . Models shown for the 3 sites in represent those at each site which simulated well the seasonality and magnitude of  $E_t$ . Gray shaded regions denote months where precipitation  $< 100$  mm.

(Fig. 5d) as water deficits (both soil and atmospheric  $D$ ) continue to rise. Comparison of the seasonality of  $g_s$  to that of LAI at a nearby ( $\sim 3$  km) site (Brando et al., 2010) revealed that the timing of the minimum in  $g_s$  at K67 lags 1 month that of LAI (Fig. 5g), and high

rates of litterfall are also coincident with increasing dry season LAI at the K67 site, implying a period of significant leaf flush. We found that a significant positive relationship ( $P < 0.05$ ) exists between  $g_s$  and LAI when  $g_s$  is lagged by one month (inset Fig. 5g), roughly the

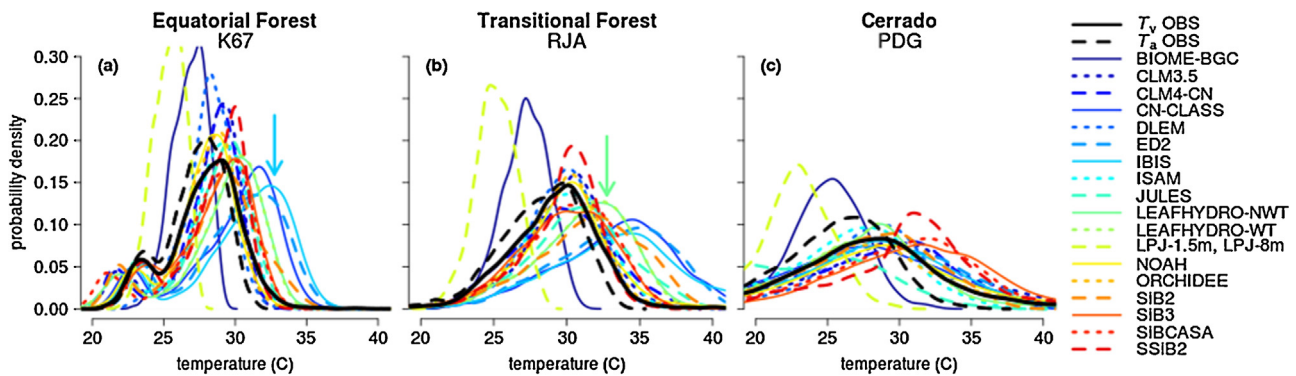


**Fig. 6.** Probability density of daytime canopy temperature ( $T_c$ ) at one site each of (a) equatorial forests (K67), (b) transitional forests (RJA), and (c) Cerrado (PDG) where canopy stomatal conductance was estimated. Observations are in black (dashed line is air temperature; solid line is the canopy aerodynamic temperature estimated from the inversion of sensible heat and aerodynamic fluxes). Colored arrows denote models (IBIS at K67 and LEAFHYDRO at RJA) which otherwise well simulate the magnitude of transpiration ( $E_t$ ) but which have warm canopy temperature biases.

amount of time required for new leaf expansion. This corroborates recent work (Restrepo-Coupe et al., 2013) which demonstrates the importance of canopy leaf flush driving the seasonality of photosynthesis across the Amazon basin. In contrast to these observations, many models which captured the seasonality of  $E$  consistently underestimated seasonal variability in  $g_s$ . Collectively, this suggests that the discrepancy between observed and modeled seasonality of vegetation water demand at equatorial and transitional forest sites K67 and RJA is due in part to such biological rhythms of leaf phenology, a process poorly represented in vegetation models.

Other models which simulated well both the seasonality and magnitude of  $E_t$  at times exhibited a systematic low bias in the magnitude of  $g_s$ . An exploration of the canopy temperatures ( $T_v$ ) of some of these models (IBIS at K67, LEAFHYDRO at RJA) revealed a corresponding warm bias (see arrows in Fig. 6). These models are able to capture the magnitude of  $E$  and  $E_t$  at these sites presumably because this warm bias contributes to a larger vapor pressure deficit in these models which, given the same atmospheric conditions, drives a larger vapor flux at low  $g_s$ . The counteracting effect of  $T_v$  bias, however, was not enough to offset more extreme biases in  $g_s$  in other models, resulting in corresponding errors in simulated  $E_t$ . For example, warm-biased models ED2 and CN-CLASS (Fig. 6a and b) consistently underestimated  $E_t$ . Finally, two models which run at a daily timestep, LPJ and Biome-BGC, use mean air temperatures to estimate leaf temperature, and as a consequence of disregarding diurnal variability in temperature and radiative heating at the leaf surface, they consistently underestimated daytime canopy temperatures at all sites (Fig. 6a–c). Simple formulations of canopy temperature using information on diurnal air temperature ranges could be readily employed to ameliorate this bias. In sum, these examples emphasize how biases in canopy temperature can have important consequences for vegetation water demand. Furthermore, models must accurately simulate vapor fluxes at the right canopy temperature because of the temperature dependency of photosynthesis (Rubisco activity, light capture) and leaf respiration.

In addition to canopy stomatal conductance, the intrinsic water use efficiency of photosynthesis ( $iWUE$ ), or photosynthesis per unit stomatal conductance, is also an important control on vegetation water demand. Higher (lower)  $iWUE$  implies vegetation is photosynthesizing at a lower (higher) internal to ambient  $CO_2$  ratio (Lloyd et al., 2002; Beer et al., 2009), and its variation across sites in Amazonia and Cerrado may reflect site differences in soil fertility, vegetation composition, or both. It is an important diagnostic for modeled  $E$  in addition to  $g_s$  because it governs how the light response of photosynthesis is translated into evaporative losses. To demonstrate the interaction between  $GPP$  and  $iWUE$  on simulated magnitudes of  $E$ , in Fig. 7 we have arrayed models in a ‘ $GPP$ – $iWUE$  space’ for select sites across the climate and vegetation composition gradient (K67, RJA, and PDG), with simulated magnitudes of transpiration ( $E_t$ ) represented by color: models in black text simulated a mean  $E_t$  within the observed mean  $E_t \pm 0.5 \text{ mm d}^{-1}$ , and models in red and blue text fell below and above this range, respectively.

Mean site  $GPP$  decreased with  $E_t$  along the climate and vegetation composition gradient from equatorial forests to Cerrado, but there was no systematic trend in  $iWUE$  across the gradient (Fig. 7). The lack of a difference in  $iWUE$  between forest and Cerrado at an annual average scale does not preclude the existence of differences in the seasonality of  $iWUE$  across sites, which we did not analyze. Still, this analysis demonstrates that site-site differences in the magnitude of  $E$  are not due to differences in  $iWUE$ ; rather, the drivers of the magnitude of  $E$  appear to be common to those controlling the magnitude of  $GPP$ . The PDG Cerrado site has a  $GPP$  (mean  $\pm$  95% confidence interval) of  $3.2 \pm 1.7 \mu\text{mol CO}_2 \text{ m}^{-2} \text{ s}^{-1}$  which is less than half that of RJA ( $7.7 \pm 1.8 \mu\text{mol CO}_2 \text{ m}^{-2} \text{ s}^{-1}$ ) or K67 ( $8.2 \pm 1.4 \mu\text{mol CO}_2 \text{ m}^{-2} \text{ s}^{-1}$ ). It is possible that the low soil

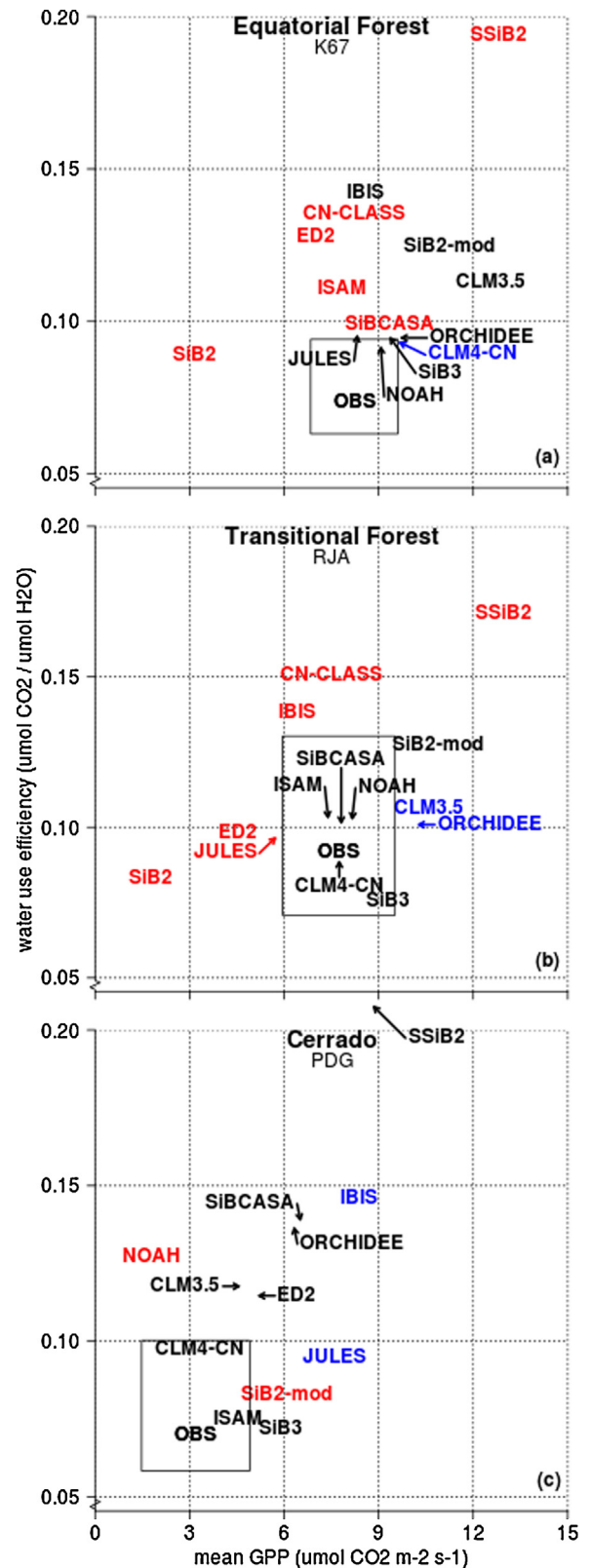


Fig. 7. Observations (“OBS”) and models plotted in intrinsic water use efficiency ( $iWUE$ )–gross primary production ( $GPP$ ) plot space with text color corresponding to modeled  $E_t$  relative to observed  $E_t$ , where red (blue) models underestimate (overestimate)  $E_t$  by at least  $0.5 \text{ mm/day } iWUE$  and  $GPP$  are the mean values observed or predicted for each site. Box represents observational error, which for  $iWUE$  is estimated as the inverse of the slopes of the 25th and 75th quantile regressions of  $g_s \sim GPP \times (h/c_a)$ .  $GPP$  error estimated as  $\pm 1$  standard deviation (For interpretation of the color information in this figure legend, the reader is referred to the web version of the article.).

**Table 4**  
Model benchmarking of the magnitude of transpiration fluxes ( $E_t$ ) across biomes with respect to vegetation demand for water. Note that mean  $E_t$  is not representative of an annual mean (see Section 2). 'High', 'low', and '✓' denote models whose mean values are greater than, less than, or within the observational error (taken as a constant 0.5 mm/day for  $E_t$ ). The last column evaluates whether models do ('✓') or do not ('x') match the observed  $E_t$ , while also matching all four observed magnitudes of vegetation demand (columns 1–4).

$g_s$	$T_v$	GPP	$iWUE$	Model	Mean $E_t$	Right $E_t$ ?	Right $E_t$ , Right demand?
<i>Equatorial forests (K34, K67, K83)</i>							
Low	✓	Low	✓	SIB2	1.92	Low	x
Low	High	✓	High	ED2	2.33	Low	x
Low	✓			HTESSSEL	2.47	Low	x
Low	✓	High	High	SSiB2	2.48	Low	x
Low	✓			LEAFHYDRO-NWT	2.53	Low	x
Low	✓			LEAFHYDRO-WT	2.61	Low	x
Low	High	✓	High	CN-CLASS	2.66	Low	x
Low	✓	✓	High	ISAM	2.72	Low	x
Low	Low	✓	✓	SIBCASA	2.99	Low	x
✓	✓	High	✓	SIB2-mod	3.18	✓	x
Low	High	✓	High	IBIS	3.19	✓	x
Low	✓	✓	High	JULES	3.20	✓	x
Low	✓	✓	High	SIB3	3.24	✓	x
Low	✓	High	High	ORCHIDEE	3.36	✓	x
✓	✓	✓	✓	<b>NOAH-MP</b>	<b>3.54</b>	✓	✓
✓	✓	✓	✓	<b>OBS</b>	<b>3.59</b>	✓	✓
High	✓	High	High	CLM35	4.07	High	x
High	✓	High	✓	CLM4-CN	4.29	High	x
<i>Transitional forest (RJA only)</i>							
Low	✓			CLM3	1.42	Low	x
Low	High	Low	✓	SIB2	1.53	Low	x
Low	High	Low	✓	ED2	2.22	Low	x
Low	✓	High	High	SSiB2	2.89	Low	x
✓	High	Low	✓	JULES	3.00	Low	x
Low	High			LEAFHYDRO-NWT	3.03	Low	x
✓	✓			HTESSSEL	3.04	Low	x
Low	High	✓	High	IBIS	3.04	Low	x
Low	High			LEAFHYDRO-WT	3.19	Low	x
Low	High	✓	High	CN-CLASS	3.20	Low	x
Low	✓	✓	✓	ISAM	3.27	✓	x
Low	✓	✓	✓	SIBCASA	3.45	✓	x
✓	✓	✓	✓	<b>OBS</b>	<b>3.73</b>	✓	✓
✓	✓	✓	✓	<b>CLM4-CN</b>	<b>3.86</b>	✓	✓
✓	✓	✓	✓	<b>NOAH-MP</b>	<b>4.01</b>	✓	✓
✓	✓	✓	✓	<b>SIB3</b>	<b>4.01</b>	✓	✓
✓	High	High	✓	SIB2-mod	4.18	✓	x
✓	✓	High	✓	ORCHIDEE	4.46	High	x
✓	✓	High	✓	CLM35	4.58	High	x
<i>Cerrado (PDG)</i>							
Low	✓	Low	Low	SIB2	0.61	Low	x
Low	✓	Low	Low	CN-CLASS	1.07	Low	x
✓	✓			CLM3	1.09	Low	x
✓	✓	High	✓	SIB2-mod	1.34	Low	x
✓	High	✓	High	NOAH-MP	1.44	Low	x
✓	✓	High	High	ED2	1.92	✓	x
✓	✓	✓	✓	<b>CLM4-CN</b>	<b>1.95</b>	✓	✓
✓	✓	✓	High	CLM35	2.00	✓	x
✓	✓			<b>LEAFHYDRO-NWT</b>	<b>2.06</b>	✓	✓
✓	High	High	High	SSiB2	2.08	✓	x
✓	✓			<b>LEAFHYDRO-WT</b>	<b>2.12</b>	✓	✓
✓	✓	✓	✓	ISAM	2.13	✓	x
✓	✓	✓	✓	<b>OBS</b>	<b>2.18</b>	✓	✓
✓	High	High	✓	SIB3	2.29	✓	x
✓	✓			<b>HTESSSEL</b>	<b>2.51</b>	✓	✓
✓	✓	High	High	SIBCASA	2.51	✓	x
✓	✓	High	High	ORCHIDEE	2.62	✓	x
✓	✓	High	High	IBIS	3.31	High	x
High	Low	High	✓	JULES	3.57	High	x

fertility of Cerrado (Furley and Ratter, 1988) combined with its substantially different species composition (Lloyd et al., 2009) places additional constraints on photosynthesis beyond those of climate alone. These additional constraints on photosynthesis are then translated into a reduced water vapor flux because  $iWUE$  did not change significantly between Cerrado and forest.

Consequently, models which failed to capture constraints on photosynthesis also had positive biases in their simulated

transpiration ( $E_t$ ). For instance, the CLM3.5 and ORCHIDEE models overestimated GPP at RJA while IBIS and JULES overestimated GPP at PDG, causing these models to overestimate water flux at these sites (Fig. 7b and c). IBIS and JULES were previously noted to “overfix” modeled  $E$  in Cerrado and it is clear that they do so by overestimating the light response of photosynthesis, i.e., GPP, as opposed to underestimating  $iWUE$ . Many otherwise well-performing models in terms of their simulated  $E_t$  were not able

to capture variations in *GPP* and *iWUE* in concert across sites. This problem was especially apparent in Cerrado, where models such as SSiB2, ORCHIDEE, SiBCASA, CLM35 and ED2 overestimated *GPP* while also overestimating *iWUE*, which allowed them to simulate the appropriate magnitude of  $E_t$ , but with the incorrect mechanisms (Fig. 7c). Overall model spread in *GPP* was greatest in the transitional forest of RJA (Fig. 7b), while model spread in *iWUE* was also large, both of which combine to explain the large model spread in simulated *E* in transitional forests (Fig. 2b). In contrast, most of the model spread in simulated *E* in equatorial forests (Fig. 2a) is due to variation in simulated *iWUE*, not *GPP*, as evidenced by the K67 site (Fig. 7a).

One of the reasons for model bias in *iWUE* can simply be attributed to parameter values in their associated stomatal closure equation (equations and parameters given in Table A3). For instance, ED2, IBIS and CNCLASS tended to overestimate *iWUE* because of lower values of  $m$ , equal to 8, 8, and 6, respectively. It should be noted that one model (ISAM) was able to capture most of the variation in the magnitude of  $E_t$  across sites with the appropriate mechanistic responses of *iWUE* and *GPP* (Fig. 7b and c). This model incorporates nutrient (nitrogen) cycles into whole-system biogeochemical processes, including photosynthesis (Jain et al., 2009) and associated stomatal responses. The CLM4-CN model, also a model incorporating nutrient cycling, also captures the variation in *E*, *iWUE*, and *GPP* across sites, except for a small positive bias in *GPP* at K34.

These results highlight the challenge facing models not to improve simulations of tropical forests at the expense of Cerrado. That Cerrado would exhibit dynamics not easily represented by models which were improved with tropical forests in mind should not be surprising; Cerrado is quite far from being analogous to seasonally dry forest both in terms of phylogenetic distance (Pennington et al., 2000; Pennington et al., 2009) and species functional traits (Hoffmann et al., 2012). Models which captured some of the biome differences in *E* as well as *GPP* and *iWUE* were models which account for nutrient limitations on forest and savanna ecophysiology, but we did not do the necessary analyses to confirm this as fact. Nevertheless, this supports recent evidence that basin-wide variation in nutrients play an important role in governing patterns in productivity (Quesada et al., 2012) and by extension, evapotranspiration. Regardless, model improvements in Cerrado and its boundary with forest will require modeling the synergistic effects of soil fertility and disturbance via fire, since these mechanisms are the primary factors controlling the relative productivity and abundance of trees and grasses at this ecotone (Furley and Ratter, 1988; Ratter, 1992).

### 3.5. Model benchmarking

We have shown that models can simulate the correct magnitude and seasonality of *E* from equatorial Amazonia to Cerrado using multiple supply and demand side mechanisms, and the observations have provided important constraints these mechanisms. A single comprehensive metric of performance for each model with respect to simulated magnitudes and seasonalities of *E* that integrates both supply and demand regulatory mechanisms is beyond the scope of this paper. However, based on our analysis of demand-side mechanisms with respect to the magnitude of  $E_t$ , we present what a model benchmark might look like in Table 4. For equatorial (K34, K67, K83), transitional (RJA only), and Cerrado (PDG) sites, models and observations are ordered by increasing magnitude of transpiration ( $E_t$ ) (not an annual mean). We then summarize whether or not models simulated with high or low bias, or within observational error, the four variables regulating vegetation water demand ( $g_s$ ,  $T_v$ , *GPP*, *iWUE*) in columns 1–4, in addition to  $E_t$  (column 7). A model which simulates a magnitude of  $E_t$  within the

observational error while also simulating the four demand variables within observational error, we deem does so “for the right reasons” (column 8), at least with respect to demand-side mechanisms regulating vegetation water demand.

Six, six, and 11 models “get the right answer” at the equatorial forest sites, the RJA transitional forest site, and the PDG Cerrado site, respectively: that is, they simulate the magnitude of  $E_t$  to within  $\pm 0.5 \text{ mm day}^{-1}$  of the observations (Table 4). At none of these sites, however, did a majority of these models do so for the right reasons. PDG was the site with the greatest number of models (five) doing so for the right reasons, but only two of these models were models which also simulated carbon fluxes. In sum, the model benchmark has identified model deficiencies which would not have otherwise been apparent based on a simple model-data comparison of evapotranspiration flux.

## 4. Conclusions

This study was undertaken to accomplish two main objectives: First, to establish how mechanisms of water supply and vegetation water demand control evapotranspiration (*E*) along a climate and vegetation composition gradient from equatorial Amazonia to Cerrado; and second, to evaluate these mechanisms in a suite of ecosystem models. Encouragingly, most models are now able to simulate with relative accuracy the magnitude and seasonality of *E* at equatorial sites and Cerrado, but transitional forests continue to pose challenges for models. However, we identified some deficiencies in models which would not otherwise be apparent based on a simple comparison of simulated and observed magnitude and seasonal cycle of *E*.

We showed that the mechanisms of upward capillary flux and deep root uptake are complementary mechanisms of water supply and can both sustain *E* during the dry season, but their relative importance is site-dependent. Some models prescribed deep roots at all sites (e.g., LPJ-8 m) or manipulated rooting depth via optimization/sensitivity analysis (e.g., BIOME-BGC, ORCHIDEE, SiB3, IBIS), while others (e.g., CLM, ISAM, NOAH-MP) relied on groundwater recharge based solely on precipitation climatology and soil texture, to make up for dry season water deficits. In contrast, the observations indicated that the relative importance of these two mechanisms did not vary as a simple function of climate or location along the climate and vegetation composition gradient. Consequently, models often simulated well the seasonality of *E*, but with the incorrect mechanism of water supply. While the real principles which govern the relative magnitude of deep root activity and capillary fluxes remain to be elucidated, contrasting the LEAFHYDRO-WT point simulations analyzed here with results from a previous study (Miguez-Macho and Fan, 2012) suggests that both the magnitude and seasonal timing of capillary fluxes is governed just as much by local topography and proximity to drainage basins as by climatology and soil texture. Capturing these effects in models, therefore, will require not only simulation of lateral subsurface water flow (a two-dimensional process), but spatial resolutions much higher than the typical GCM simulation ( $1^\circ \times 1^\circ$ ). Most importantly, however, the analysis of water supply highlights unanswered questions regarding deep root activity, both from an ecological point of view as to which trade-offs govern deep roots (as a plant trait) within and across tropical forest communities, and from a mechanistic view as to the quantity of water and nutrients transported through them.

We also showed that, while most equatorial and transitional forests demonstrated a seasonal cycle of transpiration ( $E_t$ ) which closely followed that of net radiation, vegetation water demand via canopy stomatal conductance was still a moderate to significant control. Some models, however, which simulated well the seasonal

cycle of  $E_t$  and its control by net radiation did so with near-constant canopy stomatal conductance throughout most of the year. We presented evidence at an equatorial site (Restrepo-Coupe et al., 2013) which suggests that the quantity and age distribution of leaves in the canopy plays just as significant a role in the seasonality of canopy stomatal conductance as does leaf-level stomatal control, implying that some of the data-model discrepancy is due to leaf phenology, a process poorly represented in vegetation models. Model biases in the magnitude of canopy stomatal conductance, in turn, could be related to light response ( $GPP$ ) or the intrinsic water use efficiency of photosynthesis ( $iWUE$ ), in addition to its effect on canopy temperatures. We found that most of the variation in modeled rates of  $E$  at an equatorial site was explained by  $iWUE$ , but at Cerrado, many models were characterized by a “cryptic bias”, i.e., biases in both  $iWUE$  and  $GPP$  partially cancelled each other out, leading to modeled magnitudes of  $E$  indistinguishable from the observations. While modeled  $E$  bias at the equatorial site can be remedied by a simple optimization scheme tuning the magnitude of the Ball-Berry parameter  $m$ , model issues at Cerrado would require better parameterization of both  $V_{cmax}$  (light response) and  $m$ .

Most importantly, these analyses highlight how model improvements need to focus on biological controls on  $E$  in addition to physical mechanisms, especially given the predominance of transpiration fluxes in total evapotranspiration (Jasechko et al., 2013). This will require continued and expanded efforts to monitor root and canopy demographic processes in relation to variability in available water, nutrients and light. These efforts will realize maximum benefit when conducted at sites with existing ecosystem-level eddy covariance measurement infrastructure, allowing these sub-scale processes to inform controls on ecosystem-level processes. Integrating these biological responses and feedbacks to the processes of water cycling, therefore, will improve our understanding of vegetation-climate feedbacks in the tropics.

## Acknowledgments

**Author contributions** First author B.O.C. and senior author S.R.S. designed the analyses. B.O.C. conducted the analyses. Second author N.R.C. provided BrasilFlux database support. B.O.C. and S.R.S. wrote the paper with contributions from N.R.C., P.C., J.B.F., D.G., L.G., G.M.-M., B.P., K.Sa., K.Sc., H.V., Z.-L.Y., B.K., M.H.C., and X.Z. Model output and contributions to model classification were provided by M.A.A., I.T.B., B.P.C., J.B.F., D.G., X.G., L.G., Bv.dH., K.I., H.I., A.J., N.L., G.M.-M., B.P., D.R.R., K.Sa., A.S., K.Sc., M.S., H.V. and Z.-L.Y. Key datasets and insights into their appropriate analysis were contributed by A.C.A., B.K., A.O.M., H.R.dR. and C.vR. LBA-DMIP project was coordinated by M.N.M., J.B., M.H.C., L.G.G.dG., X.Z. and S.R.S.

This research was funded by the National Aeronautics and Space Administration (NASA) (LBA investigation CD-32 and the LBA-DMIP project, award #NNX09AL52G), the National Science Foundation (Amazon-PIRE, NSF award #OISE-0730305), and the Gordon and Betty Moore Foundation's Andes-Amazon Initiative. HRdR acknowledges FAPESP (08-581203) for aiding field data collection. Soil moisture data for the RJA field site were collected under the ABRACOS project and made available by the UK Institute of Hydrology and the Instituto Nacional de Pesquisas Espaciais (Brazil). ABRACOS was a collaboration between the Agencia Brasileira de Cooperação and the UK Overseas Development Administration. B.O.C. acknowledges support from a Graduate Research Environmental Fellowship (GREF)-U.S. DOE Global Change Education Program, as well as an NSF Amazon-PIRE fellowship. J.B.F. contributed to this paper from the Jet Propulsion Laboratory, California Institute of Technology, under a contract with the National

Aeronautics and Space Administration. We thank Reto Stoeckli for initial generation of gap-filled meteorological driver data, and Enrique Rosero for discussions helping to frame some analyses for this paper. We are indebted to both LBA and ABRACOS projects, and their field technicians, without whose efforts to establish and preserve the quality of datasets used here, this paper would not have been possible. We are grateful to two anonymous reviewers whose comments greatly improved the clarity of this paper.

## Appendix A.

List of symbols, definitions, and units used in the paper (Table A1) and descriptions of the soil hydrology (Table A2) and stomatal conductance (Table A3) sub-model components for all LBA-DMIP models.

## Appendix B.

Full description of the methods used to obtain composite seasonal cycles of  $\Delta S_s$ .

## Appendix C.

A version of Fig. 3 in main text which includes the entire set of LBA-DMIP models.

## Appendix D.

Figure sets encompassing all sites and the entire set of models for the water budget analysis given in Fig. 4 of the main text.

## Appendix E. Supplementary data

Supplementary data associated with this article can be found, in the online version, at <http://dx.doi.org/10.1016/j.agrformet.2014.02.008>.

## References

- Avissar, R., Werth, D., 2004. Comments on “The regional evapotranspiration of the Amazon”. *Reply Journal of Hydrometeorology* 5 (6), 1281.
- Baker, I.T., et al., 2008. Seasonal drought stress in the Amazon: Reconciling models and observations. *Journal of Geophysical Research*, 113.
- Baldocchi, D., Luxmoore, R.J., Hatfield, J.L., 1991. Discerning the forest from the trees: an essay on scaling canopy stomatal conductance. *Agricultural and Forest Meteorology* 54, 197–226.
- Ball, J.T., Woodrow, I.E., Berry, J.A., 1987. A model predicting stomatal conductance and its contribution to the control of photosynthesis under different environmental conditions. In: Biggins, I. (Ed.), *Progress in Photosynthesis Research*. Martinus Nijhoff, Netherlands, pp. 221–224.
- Balsamo, G., et al., 2009. A revised hydrology for the ECMWF model: verification from field site to terrestrial water storage and impact in the integrated forecast system. *Journal of Hydrometeorology* 10 (3), 623–643.
- Beer, C., et al., 2009. Temporal and among-site variability of inherent water use efficiency at the ecosystem level. *Global Biogeochemical Cycles* 23 (2).
- Belk, E.L., et al., 2007. Modeling the effects of throughfall reduction on soil water content in a Brazilian Oxisol under a moist tropical forest. *Water Resources Research* 43 (8), W08432.
- Best, M.J., et al., 2011. The Joint UK Land Environment Simulator (JULES), model description—Part 1: energy and water fluxes. *Geoscientific Model Development* 4 (3), 677–699.
- Betts, R.A., et al., 2004. The role of ecosystem-atmosphere interactions in simulated Amazonian precipitation decrease and forest dieback under global climate warming. *Theoretical and Applied Climatology* 78 (1–3), 157–175.
- Bonan, G., 1998. The land surface climatology of the NCAR land surface model coupled to the NCAR Community Climate Model. *Journal of Climate* 11, 1307–1326.
- Borma, L.S., et al., 2009. Atmosphere and hydrological controls of the evapotranspiration over a floodplain forest in the Bananal Island region. *Amazonia Journal of Geophysical Research-Biogeosciences* 114, G01003.
- Brando, P.M., et al., 2010. Seasonal and interannual variability of climate and vegetation indices across the Amazon. *Proceedings of the National Academy of Sciences* 107 (33), 14685–14690.

- Bruno, R.D., da Rocha, H.R., de Freitas, H.C., Goulden, M.L., Miller, S.D., 2006. Soil moisture dynamics in an eastern Amazonian tropical forest. *Hydrological Processes* 20 (12), 2477–2489.
- Buckley, T.N., 2005. The control of stomata by water balance. *New Phytologist* 168 (2), 275–292.
- Clapp, R.B., Hornberger, G.M., 1978. Empirical equations for some soil hydraulic properties. *Water Resources Research* 14 (4), 601–604.
- Clark, D.B., et al., 2011. The Joint UK Land Environment Simulator (JULES), model description—Part 2: carbon fluxes and vegetation dynamics. *Geoscientific Model Development* 4 (3), 701–722.
- Collatz, G.J., Ball, J.T., Grivet, C., Berry, J.A., 1991. Physiological and environmental regulation of stomatal conductance, photosynthesis and transpiration: a model that includes a laminar boundary layer. *Agricultural and Forest Meteorology* 54, 107–136.
- Costa, M.H., et al., 2010. Atmospheric versus vegetation controls of Amazonian tropical rain forest evapotranspiration: are the wet and seasonally dry rain forests any different? *Journal of Geophysical Research—Biogeosciences*, 115.
- Costa, M.H., Souza, J.D.C., Ribeiro, A., 2004. Comments on “The regional evapotranspiration of the Amazon”. *Journal of Hydrometeorology* 5 (6), 1279–1280.
- Cox, P.M., Huntingford, C., Harding, R.J., 1998. A canopy conductance and photosynthesis model for use in a GCM land surface scheme. *Journal of Hydrology*, 79–94, 212–213.
- Cox, P.M., Betts, R.A., Jones, C.D., Spall, S.A., Totterdell, I.J., 2000. Acceleration of global warming due to carbon-cycle feedbacks in a coupled climate model. *Nature* 408, 184–187.
- da Rocha, H.R., et al., 2002. Measurements of CO exchange over a woodland savanna (Cerrado sensu stricto) in southeast Brazil. *Biota Tropica* 2 (1), BN01702012002.
- da Rocha, H.R., et al., 2009. Patterns of water and heat flux across a biome gradient from tropical forest to savanna in Brazil. *Journal of Geophysical Research—Biogeosciences*, 114.
- de Gonçalves, L.G.G., et al., 2013. Overview of the large-scale biosphere–atmosphere experiment in Amazonia Data Model Intercomparison Project (LBA-DMIP). *Agricultural and Forest Meteorology* 182–183, 111–127.
- de Rosnay, P., Polcher, J., 1998. Modelling root water uptake in a complex land surface scheme coupled to a GCM. *Hydrology and Earth System Sciences* 2 (2–3), 239–255.
- Dickinson, R.E., et al., 2006. The community land model and its climate statistics as a component of the community climate system model. *Journal of Climate* 19 (11), 2302–2324.
- Ducoudre, N.I., Laval, K., Perrier, A., 1993. Sechiba, a new set of parameterizations of the hydrologic exchanges at the land atmosphere interface within the lmd atmospheric general-circulation model. *Journal of Climate* 6 (2), 248–273.
- Eltahir, E.A.B., Bras, R.L., 1994. Precipitation recycling in the Amazon Basin. *Quarterly Journal of the Royal Meteorological Society* 120 (518), 861–880.
- Fan, Y., Miguez-Macho, G., 2010. Potential groundwater contribution to Amazon evapotranspiration. *Hydrology and Earth System Sciences* 14 (10), 2039–2056.
- Fisher, J.B., et al., 2009. The land–atmosphere water flux in the tropics. *Global Change Biology* 15 (11), 2694–2714.
- Foley, J.A., et al., 1996. An integrated biosphere model of land surface processes, terrestrial carbon balance, and vegetation dynamics. *Global Biogeochemical Cycles* 10 (4), 603–628.
- Furley, P.A., Ratter, J.A., 1988. Soil resources and plant communities of the central Brazilian cerrado and their development. *Journal of Biogeography* 15 (1), 97–108.
- Galbraith, D., et al., 2010. Multiple mechanisms of Amazonian forest biomass losses in three dynamic global vegetation models under climate change. *New Phytologist* 187 (3), 647–665.
- Gerten, D., Schaphoff, S., Haberlandt, U., Lucht, W., Sitch, S., 2004. Terrestrial vegetation and water balance—hydrological evaluation of a dynamic global vegetation model. *Journal of Hydrology* 286 (1–4), 249–270.
- Grant, R.F., et al., 2009. Modeling the carbon balance of Amazonian rain forests: resolving ecological controls on net ecosystem productivity. *Ecological Monographs* 79 (3), 445–463.
- Gulden, L.E., et al., 2007. Improving land-surface model hydrology: Is an explicit aquifer model better than a deeper soil profile? *Geophysical Research Letters* 34 (9).
- Harper, A.B., et al., 2010. Role of deep soil moisture in modulating climate in the Amazon rainforest. *Geophysical Research Letters*, 37.
- Hasler, N., Avissar, R., 2007. What controls evapotranspiration in the Amazon basin? *Journal of Hydrometeorology* 8 (3), 380–395.
- Haxeltine, A., Prentice, I.C., 1996. BIOME3: An equilibrium terrestrial biosphere model based on ecophysiological constraints, resource availability, and competition among plant functional types. *Global Biogeochemical Cycles* 10 (4), 693–709.
- Hodnett, M.G., Pimentel da Silva, L., da Rocha, H.R., Senna, Cruz, 1995. Seasonal soil water storage changes beneath central Amazonian rainforest and pasture. *Journal of Hydrology* 170, 233–254.
- Hoffmann, W.A., et al., 2012. Ecological thresholds at the savanna-forest boundary: how plant traits, resources and fire govern the distribution of tropical biomes. *Ecology Letters* 15 (7), 759–768.
- Huntingford, C., et al., 2008. Towards quantifying uncertainty in predictions of Amazon ‘dieback’. *Philosophical Transactions of the Royal Society B—Biological Sciences* 363 (1498), 1857–1864.
- Ichii, K., et al., 2007. Constraining rooting depths in tropical rainforests using satellite data and ecosystem modeling for accurate simulation of gross primary production seasonality. *Global Change Biology* 13 (1), 67–77.
- Jacobs, C.M.J., 1994. *Direct Impact of Atmospheric CO<sub>2</sub> Enrichment on Regional Transpiration*. Wageningen Agricultural University.
- Jain, A., et al., 2009. Nitrogen attenuation of terrestrial carbon cycle response to global environmental factors. *Global Biogeochemical Cycles* 23 (4), GB4028.
- Jarvis, P.G., 1976. The interpretation of the variations in leaf water potential and stomatal conductance found in canopies in the field. *Philosophical Transactions of the Royal Society B: Biological Sciences* 273 (927), 593–610.
- Jasechko, S., et al., 2013. Terrestrial water fluxes dominated by transpiration. *Nature* 496 (7445), 347–350.
- Juarez, R.I.N., Hodnett, M.G., Fu, R., Goulden, M.L., von Randow, C., 2007. Control of dry season evapotranspiration over the Amazonian forest as inferred from observations at a southern Amazon forest site. *Journal of Climate* 20 (12), 2827–2839.
- Krinner, G., et al., 2005. A dynamic global vegetation model for studies of the coupled atmosphere–biosphere system. *Global Biogeochemical Cycles* 19 (1), <http://dx.doi.org/10.1029/2003GB002199>.
- Lee, J.E., Oliveira, R.S., Dawson, T.E., Fung, I., 2005. Root functioning modifies seasonal climate. *Proceedings of the National Academy of Sciences of the United States of America* 102 (49), 17576–17581.
- Leuning, R., Kelliher, F.M., Depury, D.G.G., Schulze, E.D., 1995. Leaf nitrogen, photosynthesis conductance and transpiration—scaling from leaves to canopies. *Plant Cell and Environment* 18 (10), 1183–1200.
- Lloyd, J., et al., 2009. Ecophysiology of forest and savanna vegetation. In: Keller, M., Bustamante, M., Gash, J., Silva Dias, P. (Eds.), *Amazonia and Global Change*, Geophysical Monograph Series. AGU, Washington, DC.
- Lloyd, J., et al., 2002. Seasonal and annual variations in the photosynthetic productivity and carbon balance of a central Siberian pine forest. *Tellus* 54B, 590–610.
- Medvigy, D., Wofsy, S.C., Munger, J.W., Hollinger, D.Y., Moorcroft, P.R., 2009. Mechanistic scaling of ecosystem function and dynamics in space and time: ecosystem demography model version 2. *Journal of Geophysical Research* 114 (G1).
- Miguez-Macho, G., Fan, Y., 2012. The role of groundwater in the Amazon water cycle: 2 Influence on seasonal soil moisture and evapotranspiration. *Journal of Geophysical Research—Atmospheres*, 117.
- Monteith, J.L., 1995. Accommodation between transpiring vegetation and the convective boundary layer. *Journal of Hydrology* 166, 251–263.
- Nepstad, D.C., et al., 1994. The role of deep roots in the hydrological and carbon cycles of Amazonian forests and pastures. *Nature* 372 (6507), 666–669.
- Nepstad, D.C., et al., 2002. The effects of partial throughfall exclusion on canopy processes, aboveground production, and biogeochemistry of an Amazon forest. *Journal of Geophysical Research* 107 (D20).
- Niu, G.-Y., et al., 2011. The community Noah land surface model with multiparameterization options (Noah-MP): 1. Model description and evaluation with local-scale measurements. *Journal of Geophysical Research* 116 (D12).
- Oleson, K.W., et al., 2008. Improvements to the community land model and their impact on the hydrological cycle. *Journal of Geophysical Research* 113 (G1).
- Oleson, K.W., et al., 2010. Technical Description of Version 40 of the Community Land Model (CLM). National Center for Atmospheric Research, Boulder, CO, USA.
- Peak, D., Mott, K.A., 2011. A new, vapour-phase mechanism for stomatal responses to humidity and temperature. *Plant, Cell & Environment* 34 (1), 162–178.
- Pennington, R.T., Lavin, M., Oliveira, A., 2009. Woody plant diversity, evolution, and ecology in the tropics: perspectives from seasonally dry tropical forests. *Annual Review of Ecology and Systematics*, 437–457.
- Pennington, R.T., Prado, D.E., Pendry, C.A., 2000. Neotropical seasonally dry forests and quaternary vegetation changes. *Journal of Biogeography* 27 (2), 261–273.
- Poulter, B., et al., 2012. Robust dynamics of Amazon dieback to climate change with perturbed ecosystem model parameters. *Global Change Biology* 16 (9), 2476–2495.
- Quesada, C.A., et al., 2012. Basin-wide variations in Amazon forest structure and function are mediated by both soils and climate. *Biogeosciences* 9 (6), 2203–2246.
- Ratter, J.A., 1992. Transitions between Cerrado and Forest Vegetation in Brazil. In: P.A. Furley, J. Proctor and J.A. Ratter (Editors), *Nature and Dynamics of Forest-Savanna Boundaries* Chapman & Hall, London, pp 417–429.
- Restrepo-Coupe, N., et al., 2013. What drives the seasonality of photosynthesis across the Amazon basin? A cross-site analysis of eddy flux tower measurements from the Brazil flux network. *Agricultural and Forest Meteorology* 182, 128–144.
- Running, S.W., Coughlan, J.C., 1988. A general model of forest ecosystem process for regional applications I. Hydrologic balance, canopy gas exchange and primary production processes. *Ecological Modelling* 42, 125–154.
- Schaefer, K., et al., 2008. Combined simple biosphere/Carnegie-Ames-Stanford approach terrestrial carbon cycle model. *Journal of Geophysical Research* 113 (G3).
- Sellers, P.J., et al., 1996. A revised land surface parameterization (SiB2) for atmospheric GCMs. Part I: model formulation. *Journal of Climate* 9, 676–705.
- Shuttleworth, W.J., 1988. Evaporation from Amazonian rainforest. *Proceedings of the Royal Society of London, Series B Biological Sciences* 233 (1272), 321–346.
- Shuttleworth, W.J., 1991. Insight from large-scale observational studies of land atmosphere interactions. *Surveys in Geophysics* 12 (1–3), 3–30.
- Sitch, S., et al., 2008. Evaluation of the terrestrial carbon cycle, future plant geography and climate–carbon cycle feedbacks using five Dynamic Global Vegetation Models (DGVMs). *Global Change Biology* 14 (9), 2015–2039.
- Van den Hurk, B.J.J.M., Viterbo, P., Beljaars, A.C.M., Betts, A.K., 2000. Offline Validation of the ERA40 Surface Scheme. European Centre for Medium-Range Weather Forecasts.
- Verbeeck, H., et al., 2011. Seasonal patterns of CO<sub>2</sub> fluxes in Amazon forests: fusion of eddy covariance data and the ORCHIDEE model. *Journal of Geophysical Research* 116 (G2).

- Verseghy, D.L., 1991. CLASS—A Canadian Land Surface Scheme for GCMs. 1. Soil model. *International Journal of Climatology* 11 (2), 111–133.
- Victoria, R.L., Martinelli, L.A., Mortatti, J., Richey, J., 1991. Mechanisms of water recycling in the Amazon Basin— isotopic insights. *Ambio* 20 (8), 384–387.
- Walker, G.K., Sud, Y.C., Atlas, R., 1995. Impact of the ongoing amazonian deforestation on local precipitation—a GCM simulation study. *Bulletin of the American Meteorological Society* 76 (3), 346–361.
- Werth, D., Avissar, R., 2002. The local and global effects of Amazon deforestation. *Journal of Geophysical Research-Atmospheres* 107 (D20).
- Zeng, X., Decker, M., 2009. Improving the numerical solution of soil moisture-based Richards equation for land models with a deep or shallow water table. *Journal of Hydrometeorology* 10, 308–319.
- Zhan, X., Xue, Y., Collatz, G.J., 2003. An analytical approach for estimating CO<sub>2</sub> and heat fluxes over the Amazonian region. *Ecological Modelling* 162 (1–2), 97–117.